NEUTRON FORM FACTORS FROM ELASTIC ELECTRON-DEUTERON SCATTERING RATIO EXPERIMENTS AT VERY LOW MOMENTUM TRANSFERS

Raymond William Berard

NAVAL POSTGRADUATE SCHOOL
Monterey, California

THESIS

NEUTRON FORM FACTORS FROM ELASTIC - ELECTRON-DEUTERON SCATTERING RATIO EXPERIMENTS AT VERY LOW MOMENTUM TRANSFERS

by

Raymond William Berard
and
Timothy Joseph Traverso

Thesis Advisors: F.R. Buskirk
X.K. Maruyama

June 1973

Approved for public release; distribution unlimited.

Neutron Form Factors from

Elastic Electron-Deuteron Scattering Ratio Experiments

at Very Low Momentum Transfers

by

Raymond William Berard
Ensign, United States Navy
B.S., United States Naval Academy, 1972

and

Timothy Joseph Traverso
Ensign, United States Navy
B.S., United States Naval Academy, 1972

Submitted in partial fulfillment of the
requirements for the degree

MASTER OF SCIENCE IN PHYSICS

from the

NAVAL POSTGRADUATE SCHOOL
June 1973

ABSTRACT

Measurements of the ratio of the elastic electron-deuteron scattering cross section to the elastic electron-proton scattering cross section were made for low momentum transfers. Augmented by the work of Topping [5], these data span a range of q^2 from 0.05 fm^{-2} to 0.50 fm^{-2}. From these, the electric form factor of the neutron, G_{E_n}, was extracted using three Lomon-Feshbach wave functions for the deuteron, (LF1, LF5, and LF15). Values of the slope of G_{E_n} versus q^2 were measured to be 0.0218 ± 0.0022 for LF1, 0.0220 ± 0.0022 for LF5, and 0.0185 ± 0.0022 for LF15. Although the data seems to prefer model LF15, all were found to be in agreement with the thermal neutron-electron slope of 0.0193 ± 0.0004. The root mean square structure radius of the deuteron was also extracted, using a method devised by Schumacher, and was found to be 1.9665 ± 0.0045 fm. Relativistic corrections proposed by Casper and Gross [6, 18] were compared with the relativistic correction of Friar [8] and no significant differences were found in the region investigated.

TABLE OF CONTENTS

LIST OF TABLES

LIST OF FIGURES

ACKNOWLEDGMENTS

We wish to express our heartfelt gratitude to our thesis co-advisors, Professor X. K. Maruyama and Professor F. R. Buskirk for their encouragement and willing assistance through long hours of data acquisition and analysis. Their theoretical insights and experimental experience helped us greatly through this work.

Thanks are also extended to Professors J. N. Dyer and E. B. Dally for their assistance in both data taking and a most useful introduction to the theory of electron scattering.

To Mr. H. McFarland and Mr. D. Snyder go our thanks for contributions of time and technical skills in redesigning the counting system and in generally keeping the LINAC running.

Finally, we would like to thank our wives, Marilyn Traverso and Kathleen Berard, for their continuing support, encouragement and understanding throughout our work here. Also we wish to thank Kathy for the hours she spent typing our many drafts.

I. INTRODUCTION

The deuteron being composed of one proton and one neutron is the only stable two body nucleus and, as such, is the simplest of the nuclei except for the hydrogen nucleus. The proton exists as a stable particle in the form of a hydrogen nucleus, but the isolated neutron is unstable. In order to obtain information concerning the neutron, this work will compare electron scattering from the deuteron and proton and extract the electric form factors of the neutron, G_{E_n}, which gives information on the charge structure of the neutron.

This experiment measured G_{E_n} at various values of q^2 (the square of the Lorentz invariant four-momentum transferred from the scattered electron to the target nucleus) ranging from 0.4 fm^{-2} to 0.5 fm^{-2}, in order to resolve differences among several earlier experiments [1,2,3,4]. The results of this work augmented with those of Topping [5] provide values of the neutron charge form factor for the momentum range q^2 = 0.05 fm^{-2} to 0.50 fm^{-2}. By comparing these G_{E_n}, which are obtained with the use of several different wave functions, to the G_{E_n} predicted by the very accurate thermal neutron experiment of Krohn and Ringo [4], a model that best represents the structure of the deuteron may be found. Three different models containing D-state contributions of 4.57, 5.20 and 7.55% were tested and

although the results are not conclusive, the data favors the model with 7.55% D-state. Two different relativistic corrections were investigated, the first developed by Gross [6] and modified by Schumacher [7] and the second developed by Friar [8]. Results using both methods are reported here. For the momentum transfers of this experiment, it is shown that the differences between the two methods are negligible. From the slopes of G_{E_n} for the various deuteron models used, a mean structure radius of the deuteron is extracted employing a method developed by Schumacher [7].

The organization of this thesis is as follows: the concepts of electron scattering and the definitions of terms needed to describe the scattering from protons and deuterons are contained in Chapter II.

Chapter III discusses briefly the experimental equipment and the procedures followed in order to obtain the data.

The contents of Chapter IV discusses the methods employed for data reduction. Included are discussions of corrections and normalizations made to the data, radiative and ionization corrections to the scattering spectra, and a detailed analysis of the sources of errors.

Chapter V presents the results using several different wave functions and both methods for incorporating the relativistic correction. Plots for G_{E_n} versus q^2 are included for all cases. Also included is a Rosenbluth Plot as an experimental verification of the conventional scaling law assumptions of Chapter II.

Chapter VI presents the conclusions of this work and recommendations by the authors for future experiments. Five appendices amplify details of several topics discussed in this thesis. The last appendix is a compilation of the FORTRAN codes used in the data analysis.

II. THEORY

A. NEUTRON CHARGE FORM FACTOR

The cross section for an extremely relativistic electron scattering from a spinless point nucleus with no magnetic moment has been calculated by Mott [9],

$$\sigma_M(\theta) = \left(\frac{d\sigma}{d\Omega}\right)_{Mott} = \left\{\frac{Ze^2}{2E_i}\right\}^2 \frac{\cos^2\frac{\theta}{2}}{\sin^4\frac{\theta}{2}} \frac{1}{\xi} , \qquad \text{(II-1)}$$

where

$$\xi = 1 + \frac{2E_i}{M_n c^2} \sin^2\frac{\theta}{2}$$

is the recoil factor.

The experimental cross section is related to the Mott cross section by

$$\left(\frac{d\sigma}{d\Omega}\right)_{exp} = \left(\frac{d\sigma}{d\Omega}\right)_{Mott} G^2(q^2) ,$$

where $G(q^2)$ is the total form factor of the nucleus, which in the case of charge scatterings is a function only of the square of the four-momentum transfer. The form factor takes into account the finite extent of the nucleus.

A theoretical expression for the experimental cross section for a proton has been developed by Rosenbluth [10] and is given in terms of the Mott cross section and total form factor G_p^2 as developed by Hand, et al. [11]

$$\frac{d\sigma}{d\Omega} = \sigma_M^p(\theta)\ G_p^2 \ , \qquad \text{(II-2)}$$

where $\sigma_M^p(\theta)$ is the proton Mott cross section and

$$G_p^2 = \frac{G_{E_p}^2 + \tau\ G_{M_p}^2}{1 + \tau} + 2\tau\ \tan^2\frac{\theta}{2}\ G_{M_p}^2 \ ,$$

where G_{E_p} and G_{M_p} are the electric and magnetic form factors of the proton respectively and $\tau = \frac{q^2}{4M_p^2}$.

In principle, Equations II-1 and II-2 may be used to measure G_{E_p} and G_{M_p} by doing experiments at constant q with various values of incident energy and scattering angle. However, for low values of q, the magnetic term is small (at most 15% of the total) so that it is more convenient to calculate the magnetic scattering using the scaling law developed by Lehmann et al. [12] and others [11], which was shown to be valid at low momentum transfers by Brooks and Sessler [13]. In terms of the proton magnetic moment, μ_p, the scaling law is given by

$$G_{M_p} = \mu_p\ G_{E_p} \ . \qquad \text{(II-3)}$$

Utilizing Equation II-3, Equation II-2 can be simplified to

$$G_p^2 = \frac{G_{E_p}^2}{1+\tau}\left[1 + \tau\mu_p^2\left\{1 + 2(1+\tau)\ \tan^2\frac{\theta}{2}\right\}\right] \ . \qquad \text{(II-4)}$$

Since the $\tau\mu_p^2$ term in the brackets is due only to magnetic factors, defining $C_p = \tau\mu_p^2\{1+2(1+\tau)\tan^2\frac{\theta}{2}\}$, equation II-4 can be written

$$G_p^2 = \frac{G_{E_p}^2}{1+\tau}\,[1+C_p] \ ,$$

Rewriting this and defining a proton magnetic correction term, $K_M^p = \frac{1+\tau}{1+C_p}$, an expression for $G_{E_p}^2$ is found,

$$G_{E_p}^2 = G_p^2\, K_M^p \ . \qquad \text{(II-5)}$$

From Equation II-2, it can be seen that G_p^2 can be obtained from the ratio of the experimental cross section to the Mott cross section and, $G_{E_p}^2$ can be written in terms of measurable quantities.

$$G_{E_p}^2 = \frac{\frac{d\sigma^p}{d\Omega}}{\sigma_M^p(\theta)}\, K_M^p \qquad \text{(II-6)}$$

An analogous method is used to develop an expression for $G_{E_d}^2$, the electric form factor of the deuteron. Jankus has developed an expression for the cross section for electron scattering from the deuteron [14]. Written in a form that includes form factors to account for the finite extent of the nucleons, Jankus' results [15] are

$$\frac{d\sigma^d}{d\Omega} = \sigma_M^d(\theta)\left\{G_{E_d}^2(q^2) + \frac{8}{9}\,\eta^2 G_{Q_d}^2(q^2) + \frac{2}{3}\,G_{M_d}^2(q^2)\left[1+2(1+\eta)\tan^2\frac{\theta}{2}\right]\right\}, \qquad \text{(II-7)}$$

where $\eta = \frac{q^2}{4M_d^2}$ and $G_{E_d}(q^2)$, $G_{Q_d}(q^2)$, $G_{M_d}(q^2)$ are respectively the charge, quadrupole and magnetic moment form factors of the deuteron. They are given by:

$$G_{E_d} = (G_{E_p} + G_{E_n})\, C_E \ , \quad G_{Q_d} = (G_{E_p} + G_{E_n})\, C_Q \ ,$$

$$G_{M_d} = 2 \frac{M_d}{M_p} \left\{ (G_{E_p} + G_{E_n}) C_L + (G_{M_p} + G_{M_n}) C_S \right\}.$$

Here, C_E is the charge structure factor, C_Q is the quadrupole structure factor, C_L accounts for the magnetic contribution to scattering arising from charge convection in the deuteron and C_S explains the contribution to scattering by the magnetic moments of the proton and neutron. These four factors C_E, C_Q, C_L, and C_S are all model dependent in that they arise from integrals involving S and D state wave functions of the deuteron [5]. Values for C_E, C_Q, C_L, and C_S for momentum transfers studied were supplied by Lomon [16] for the Lomon-Feshbach Models LF1, LF5 and LF15 [17] which contain percent D-state contributions of 4.57, 5.20, and 7.55 respectively.

If u(r) and w(r) are the normalized S and D-state wave functions, then C_E is given by

$$C_E = \int_o^\infty [u^2(r) + w^2(r)] \, j_o \left(\frac{qr}{2}\right) dr ,$$

where j_o is a spherical Bessel function, corresponding expressions for C_Q, C_L, and C_S may be found in Ref. [39]. In the static limit (q=0), the above functions are given by

$$G_{E_d}(0) = 1 , \qquad G_{Q_d}(0) = M_d^2 Q,$$

$$G_{M_d}(0) = \frac{M_p}{M_d} \left[\mu_p + \mu_n - \frac{3}{2} P_D \left(\mu_p + \mu_n - \frac{1}{2} \right) \right] ,$$

$$C_E(0) = 1, \qquad C_Q(0) = M_d^2 Q ,$$

$$C_S(0) = 1 - 3/2 \, P_D , \qquad C_L(0) = 3/2 \, P_D ,$$

where Q is the quadrupole moment of the deuteron, μ_p and μ_n are the proton and neutron magnetic moments respectively, and $P_D = \int_o^\infty w^2(r)dr$ is the D-state probability of the deuteron.

Relativistic corrections to the deuteron scattering problem have been calculated by Gross [6], and Casper and Gross [18] and Friar [8]. These corrections account for relativistic modifications of the deuteron wave functions and the nucleon current incorporating not only Lorentz contraction in two dimensions, but also the fact that the equal-time wave function in the rest frame is not the same as the equal time wave function in the moving frame.

Schumacher and Bethe [7] and Elias et al. [15] have shown that the relativistic corrections of Casper and Gross [6,18] to the deuteron form factors, to order $\frac{q^2}{4M_p^2}$, enter as a factor $(1-\frac{\tau}{2})^2$ on the right hand side of Equation II-7.

Friar has shown that the relativistic correction enters in two ways; first, a factor $(1+\tau)^{-1}$ should multiply the right hand side of Equation II-7; second, C_E must be evaluated at an effective $q^{2'} = q^2/(1+\eta)$. A comparison of the results using both formulations may be found in Section V.

In Appendix D, it is shown that by expanding Friar's correction in a binomial series for low q^2, Schumacher's correction differs by less than 4 parts in 10^4 for the highest q^2 investigated. Consequently, the change in C_E is negligible at low q^2. The relativistic corrections of Casper and Gross [18] in the form developed by Schumacher [7] are used in this work.

When Equation II-7 is used to analyze the deuteron experiments, a scaling law for G_{M_d} is used [3].

$$G_{M_d} = \mu_d \frac{M_d}{M_p} G_{E_d}$$

The quadrupole term is dropped since it is less than 5×10^{-4} in comparison to the total at the highest value of q^2 reached in this experiment [38]. Equation II-7 may be written in the form

$$\frac{d\sigma^d}{d\Omega} = \sigma_M^d(\theta) \left\{ G_{E_d}^2 + \frac{2}{3} \mu_d^2 G_{E_d}^2 \tau \left[1+2(1+\eta) \tan^2 \frac{\theta}{2} \right] \right\} (1 - \frac{\tau}{2})^2 .$$

Defining $C_d = \frac{2}{3} \tau \mu_d^2 \left[1+2(1+\eta) \tan^2 \frac{\theta}{2} \right]$ and noting that

$$\frac{d\sigma^d}{d\Omega} = \sigma_M^d(\theta) \; G_d^2 ,$$

where G_d is the total form factor of the deuteron, then

$$G_d^2 = (G_{E_p}^2 + G_{E_n}^2) \; C_E \; (1 + C_d)(1 - \frac{\tau}{2})^2 . \qquad \text{(II-8)}$$

Additionally, by defining $K_{M_r}^d$ as the deuteron magnetic and relativistic correction factor, the following is obtained:

$$K_{M_r}^d = \frac{1}{1+C_d} \left(\frac{1}{1-\tau/2} \right)^2 .$$

From Equation II-8, the deuteron electric form factor, G_{E_d}, is obtained in terms of $K_{M_r}^d$;

$$G_{E_d}^2 = G_d^2 \, K_{M_r}^d = \frac{\frac{d\sigma^d}{d\Omega}}{\sigma_M^d(\theta)} K_{M_r}^d = (G_{E_p} + G_{E_n})^2 \; C_E^2 . \qquad \text{(II-9)}$$

The ratio of the proton and deuteron electric form factors, is expressed in terms of G_{E_n} and G_{E_p} as

$$\frac{G_{E_d}(q_d^2)}{G_{E_p}(q_p^2)} = \frac{(G_{E_p}(q_d^2) + G_{E_n}(q_d^2))}{G_{E_p}(q_p^2)} C_E^2. \qquad \text{(II-10)}$$

Combining Equations II-6, and II-9, with Equation II-10, the ratio in Equation II-10 can be written in terms of measured quantities only.

$$\frac{[G_{E_p}(q_d^2) + G_{E_n}(q_d^2)]\, C_E}{G_{E_p}(q_p^2)} = \left[K^d_{M_r} \frac{\frac{d\sigma^d}{d\Omega}}{\sigma^d_M(\theta)}\right]^{\frac{1}{2}} \left[K^p_M \frac{\frac{d\sigma^p}{d\Omega}}{\sigma^p_M(\theta)}\right]^{-\frac{1}{2}} \qquad \text{(II-11)}$$

It is important to note that q_d and q_p, which are the four momenta transferred to the deuteron and proton respectively have different values. The incident energy was adjusted to make the final electron energies from both the deuteron and proton scatterings equal. This insures that the transmission efficiency of the spectrometer and the detector efficiencies were constant for both gases, but the four momentum transfers were slightly different. The deVries b' fit [19] for the proton electric form factor was used to adjust for this slight difference in momentum transfers.

$$G_{E_p}(q_d^2) = G_{E_p}(q_p^2) \left\{\frac{G_{E_p}(q_d^2)}{G_{E_p}(q_p^2)}\right\}_{\text{deVries}}. \qquad \text{(II-12)}$$

The ratio in Equation II-11 may be written

$$\frac{G_{E_p}(q_d^2) + G_{E_n}(q_d^2)}{G_{E_p}(q_d^2)} = \frac{1}{C_E}\left(\frac{\frac{d\sigma^p}{d\Omega}}{\frac{d\sigma^p}{d\Omega}}\,\frac{\sigma_M^p(\theta)}{\sigma_M^d(\theta)}\,\frac{K_{M_r}^d}{K_M^p}\right)^{\frac{1}{2}}\left\{\frac{G_{E_p}(q_p^2)}{G_{E_p}(q_d^2)}\right\}_{deVries}.$$

Solving this for $G_{E_n}(q_d^2)$ yields:

$$G_{E_n}(q_d^2) = G_{E_p}(q_d^2)\left\{\left(\frac{R_{exp}}{R_{Mott}}\,\frac{K_{M_r}^d}{K_M^p}\right)^{\frac{1}{2}}\left\{\frac{G_{E_p}(q_p^2)}{G_{E_p}(q_d^2)}\right\}_{deVries}\frac{1}{C_E} - 1.0\right\} \quad \text{(II-13)}$$

R_{exp} is the experimental ratio of the deuteron cross section to the proton cross section, and R_{mott} is the ratio of $\sigma_M^d(\theta)$ to $\sigma_M^p(\theta)$. Note that $\sigma_M^p(\theta)$ and K_M^p were calculated at the incident energy of the electron on the hydrogen, which was slightly higher than the energy of the electrons on the deuterium.

Writing

$$\left(\frac{G_{E_d}}{G_{E_p}}\right)^2 = \frac{R_{exp}}{R_{Mott}}\,\frac{K_{M_r}^d}{K_M^p}\left\{\frac{G_{E_p}(q_p^2)}{G_{E_p}(q_d^2)}\right\}_{deVries},$$

Equation II-13 can be rewritten in the more convenient form,

$$G_{E_n}(q_d^2) = \left\{\frac{G_{E_d}}{G_{E_p}}\,\frac{1}{C_E} - 1.0\right\} G_{E_p}(q_d^2). \quad \text{(II-14)}$$

In this form $G_{E_n}(q_d^2)$ includes the effects of the Gross relativistic corrections to the deuteron form factor.

B. NEUTRON ROOT MEAN SQUARED CHARGE RADIUS

In the Breit or "brickwall" frame, the form factors G_{E_n} and G_{M_n} can be separated. The Breit frame is the

reference frame in which the incident and final electron energies are equal, and the initial and final momenta of the deuteron are equal but oppositely directed [20].

In this frame $G_{E_n}(q^2)$ is the Fourier transform of the charge distribution [21,22] and can be written as

$$G_{E_n}(q^2) = \int_0^\infty \rho(r)\, e^{i\vec{q}\cdot\vec{r}}\, d^3\vec{r} \ .$$

The exponential term may be expanded in a power series about $q^2 = 0$ and the coefficients of q^n are the n^{th} moments of the charge distribution. For symmetric charge distributions, only the even moments are non-zero. G_{E_n} is given by

$$G_{E_n}(q^2) = G_{E_n}(0) - \frac{1}{6}\langle r_{CH}^2\rangle\, q^2 + \frac{\langle r_{CH}^4\rangle q^4}{120} + \ldots, \qquad \text{(II-15)}$$

where $\langle r_{CH}^2\rangle$ is the mean square charge radius of the charge distribution. The slope of G_{E_n} as a function of q^2 for low momentum transfers is related to the mean square neutron charge radius by

$$\frac{d}{dq^2} G_{E_n} = -\frac{1}{6}\langle r_{CH}^2\rangle \ .$$

III. EXPERIMENTAL EQUIPMENT AND PROCEDURE

A. NAVAL POSTGRADUATE SCHOOL ELECTRON LINEAR ACCELERATOR

The 100 MeV NPS LINAC is an electron accelerator similar in design to the Stanford University Mark III linear accelerator described by Chodorow et al. [23]. The thirty foot accelerator is powered by three Klystrons, each of which receives up to twenty-two megawatts of peak power. The beam energy may be varied from 30 to 105 MeV with an average maximum current of about 1μA. The machine is pulsed at a rate of 60 pulses per second, and each pulse is about one microsecond in duration.

The beam energy is selected by the beam deflection magnets and energy defining slits. The field of these magnets is measured by a nuclear magnetic resonance (NMR) probe. With the aid of quadrupole magnets, the beam is focused to a beam diameter of about 2 mm at the target. A detailed description of the NPS LINAC is given by Barnett and Cunneen [24].

B. SPECTROMETER AND COUNTING SYSTEM

The spectrometer, described in detail by Oberdier [25], is a movable 120°, 16 inch radius, double-focusing magnetic spectrometer able to detect electrons scattered at angles between 45° and 150° in steps of 15°. Ten NE102 plastic scintillation counters span part of the focal plane of the spectrometer, where each detector serves as the source of a

counting channel. The width of the counters allows a momentum spread, $\Delta p/p$, of about 0.3% for each channel. Two large detectors, spanning the same field as the ten smaller detectors, served as dual coincidence backing counters. Thus an electron passing through both backing detectors and a front detector will register as one count on the Jorway Model 1836 Dual Channel Scaler located in the control room. A triple coincidence pulse will register on a scaler only if it occurs during the time that the counter gating circuit, gated with the accelerator gun pulse, is open. This prevents background counts from registering between electron-beam pulses.

Scalers are capable of recording periodic pulses up to 150 MHz, but due to the pulsed nature of the beam, the count rate was held below 60 counts/sec on all runs to avoid large count rate losses. The count rate correction was found to be linear up to 100 counts/sec and is applied in the codes BERHFORM and TRADFORM. It was decided to use only counters 4 through 7 in order to consistently follow Topping's [5] procedure since the data points accumulated by Topping were used in the present work. Sufficient data were taken such that the ratios found from channels 4 through 7 were well defined.

The gas target cell used was a two inch diameter steel cylinder with 1.0 mil Havar windows positioned to allow the incident electrons to enter and the scattered electrons to exit. Both the H_2 and D_2 gases were maintained at liquid

nitrogen temperature and about 150 psig. The gas target system is described in detail by Topping [5].

C. DATA ACCUMULATION

Before entering into the actual procedure for obtaining data several terms must be defined. A "point" is the set of data obtained at one spectrometer setting for either the proton or deuteron. It consists of the number of counts registered in each of the ten counters, the integration capacitance and voltage, machine and spectrometer energies and the time required to take the data. A "peak" is the collection of data associated with one of the ten channels, e.g., "peak 4" refers to the data collected by counter number 4. A "run" is the collection of all the points of all the peaks for both the deuterium and hydrogen at one value of q^2 and scattering angle.

Topping [5] reported results of 21 runs from $q^2 = 0.05$ fm^{-2} to 0.35 fm^{-2}. The results of his runs and the 12 runs made by the authors will be combined to extend the data set to .05 fm^{-2}. The data collected by the authors were mainly obtained under the same conditions and same methods as used by Topping [5].

All data for each point were recorded automatically (see Section IV-A). A run consisted of between 50 and 75 points first taken with hydrogen in the target and then repeated with deuterium.

The spectrometer was first "saturated" at a field value corresponding to an electron energy of 100 MeV before data

were taken on either H_2 or D_2 to insure that the same hysteresis loop was followed on both spectra. The spectrometer was then set such that the elastic scattering spectrum was well above channel 4. The energy selected by the spectrometer was stepped down 0.05 MeV between each point. This process was continued until the energy selected by the spectrometer was about two full widths at half maximum below peak 7. Both the H_2 and D_2 spectra were obtained in the same manner.

Two additional bits of data were recorded by hand, the Secondary Emission Monitor (SEM) efficiency and the pressure in the gas target. The SEM efficiency was measured when each of the peaks registered a maximum number of counts; therefore, a total of eight values were taken for each run and they varied less than 0.1%.

The above data were always taken under conditions that were as similar as possible for the deuteron and the proton. The authors made runs from $q^2 = 0.4$ fm^{-2} to 0.5 fm^{-2}. The time required to complete a run in this experiment was greater than for the experiment of Topping because of the decrease of the cross section with q^2, and the fact that back angles had to be used exclusively. Consequently H_2 and D_2 spectra were accumulated on two successive days. This was a deviation from Topping's procedure, but this method gave data that reproduced within statistics.

The beam charge integration was always set such that the hydrogen peaks contained from 10,000 to 20,000 counts in a single channel.

As in Ref. [5], this work eliminates the need for counter efficiencies by calculating a ratio of $\frac{d\sigma^d}{d\Omega} / \frac{d\sigma^p}{d\Omega}$ for each channel.

IV. DATA ANALYSIS

A. DATA REDUCTION

The data collected on a Model 33 teletype was transcribed onto computer data cards compatible for use on the IBM 360-C. The data cards were organized such that there were two cards for every point obtained at a given spectrometer setting. The first card contained the counts for each of the ten counters, and the second contained the number of background counts, the integration time, incident electron energy, the voltage integration, the energy setting for the spectrometer, the capacitor setting, and the integrated beam charge as measured by the SFM. The hydrogen and deuterium data were treated separately with FORTRAN programs BERHFORM and TRADFORM respectively which are listed in Appendix E. These programs are rivised versions of TOP#FORM [5]. They are used primarily to calculate the cross section measured by channels 4 through 7, but they also make count rate corrections and charge monitor normalizations. Charge monitor normalization was required because the automatic termination of the integration for each of the spectrometer settings did not always stop the counting system at the same value of beam charge. The correction was

$$N(\text{normalized}) = N(\text{actual}) \frac{V_{\text{reference}}}{V_{\text{actual}}} \qquad \text{(IV-1)}$$

where V_{actual} is the actual voltage at the end of integration and $V_{reference}$ is an arbitrary standard voltage used to normalize the hydrogen and deuterium counts.

These programs were also used to plot the normalized count rate corrected spectra on the CALCOMP plotters at the NPS Computer Center. For the first plotting run, certain additional data, which are necessary to calculate cross sections, (such as the radiation corrections and densities) were given arbitrary values. The count-rate corrected and normalized counts for both deuterium and hydrogen peaks were plotted. Using these plots, the position of each peak and the line shape of the electron spectrum was visually determined. A smooth curve was fit through the points and those points that were affected by energy instabilities were appropriately adjusted. Typical plots of both raw data and smoothed curves are reproduced in Figures IV-1, IV-2, IV-3 and IV-4.

The radiation correction program TOPRADCR [5] requires the following inputs: 1) the peak energies; 2) the pressure in the gas target for hydrogen and deuterium; and 3) ΔE which is the integration interval from the peak energy to the final spectrometer setting at which data was taken. These data were obtained from the before mentioned plots. TOPRADCR also used the composition and thickness of the gas target windows and the virial coefficients of hydrogen and deuterium as stored constants. TOPRADCR calculated the Schwinger radiation, bremsstrahlung and Landau ionization corrections along with the density of the gas for each channel (peak). The necessity for the radiation corrections will be discussed later in Section IV-C. Average background was determined from the spectrum above the elastic peak.

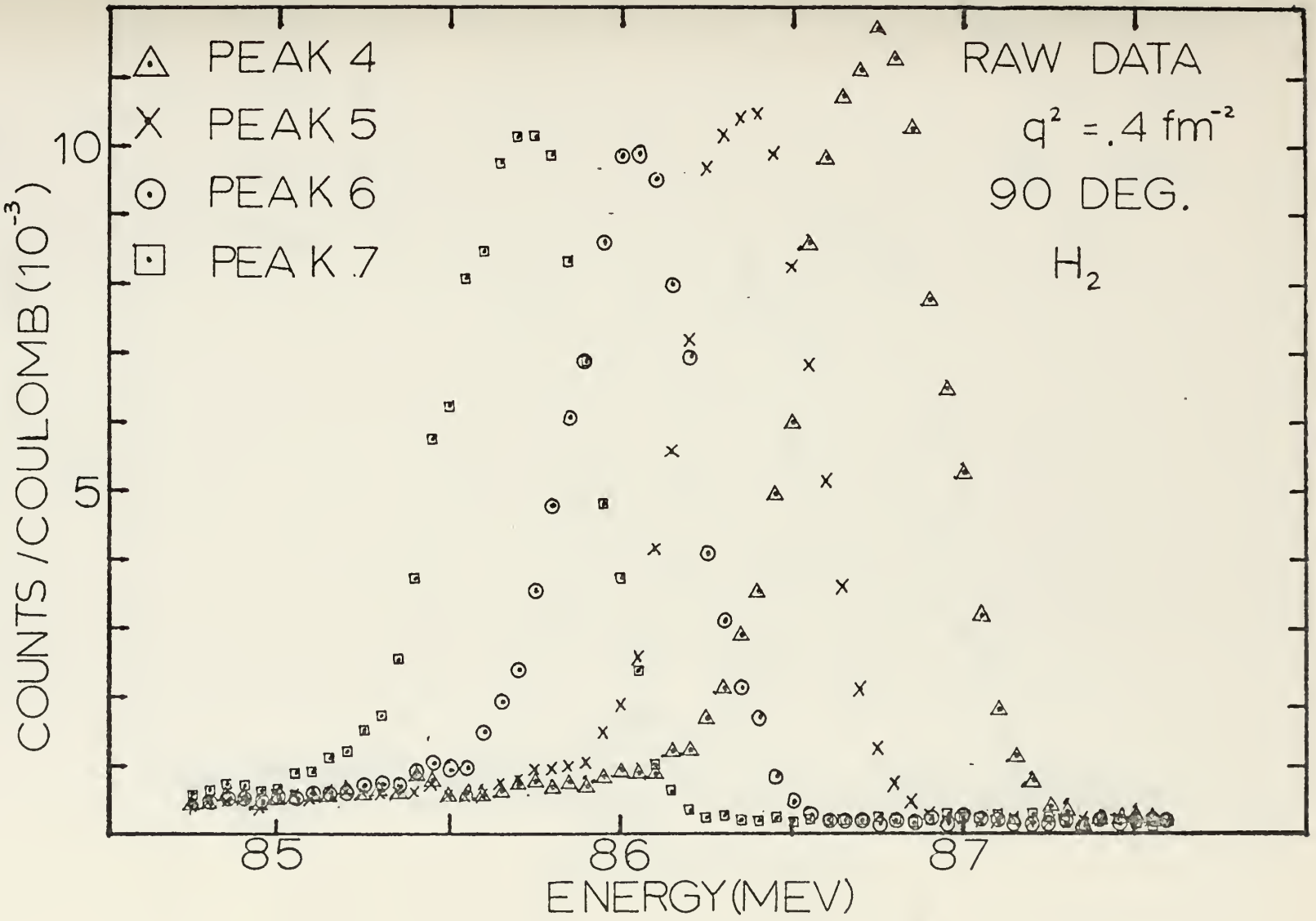
PEAK 4
PEAK 5
PEAK 6
PEAK 7
RAW DATA
$q^2 = .4\ fm^{-2}$
90 DEG.
H_2
COUNTS / COULOMB (10^{-3})
10
5
85
86
87
ENERGY (MEV)

Figure IV-1

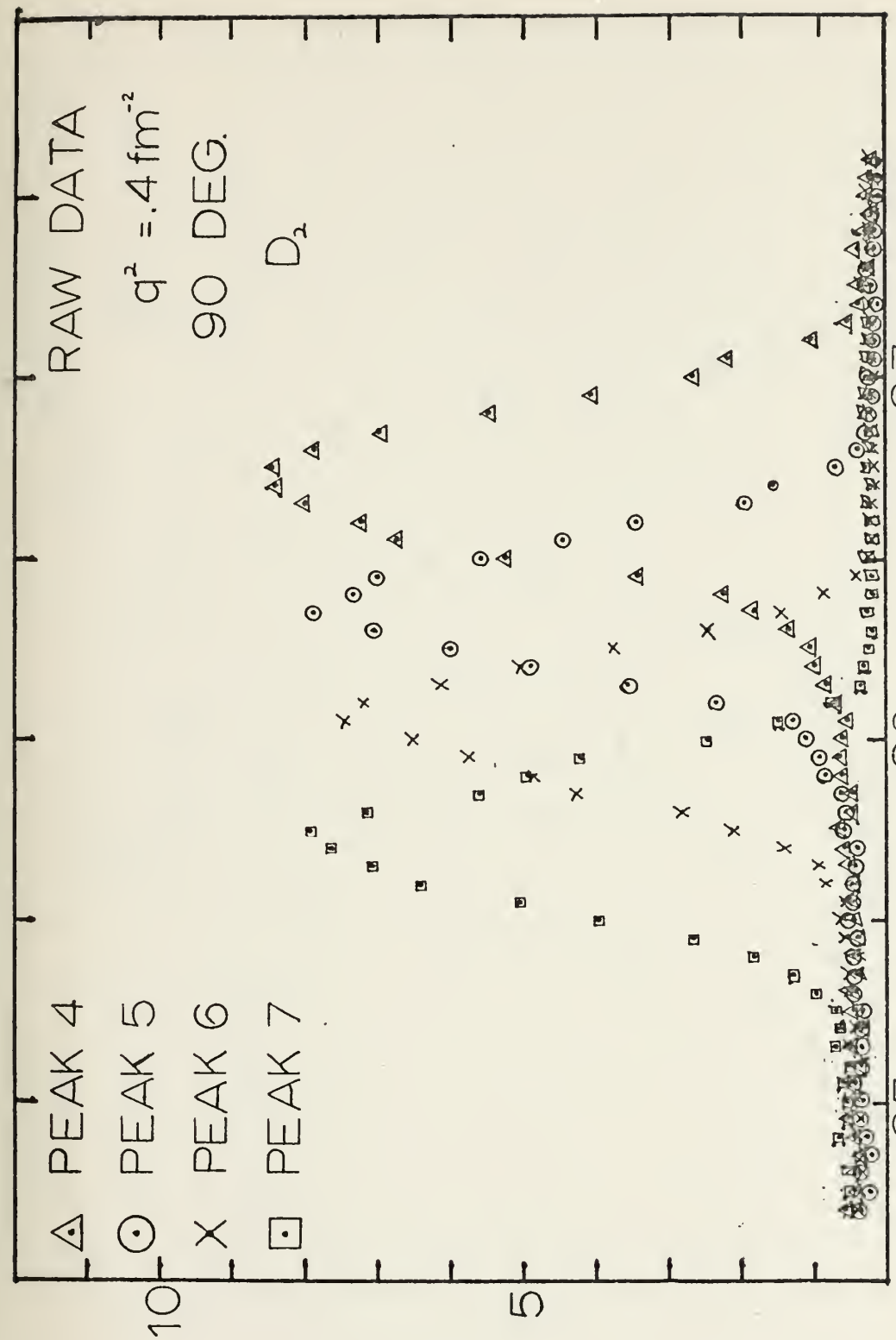
RAW DATA
$q^2 = .4\ fm^{-2}$
90 DEG.
D_2
△ PEAK 4
⊙ PEAK 5
× PEAK 6
⊡ PEAK 7
10
5
85
86
87
ENERGY (MEV)
COUNTS/COULOMB (10^3)

Figure IV-2

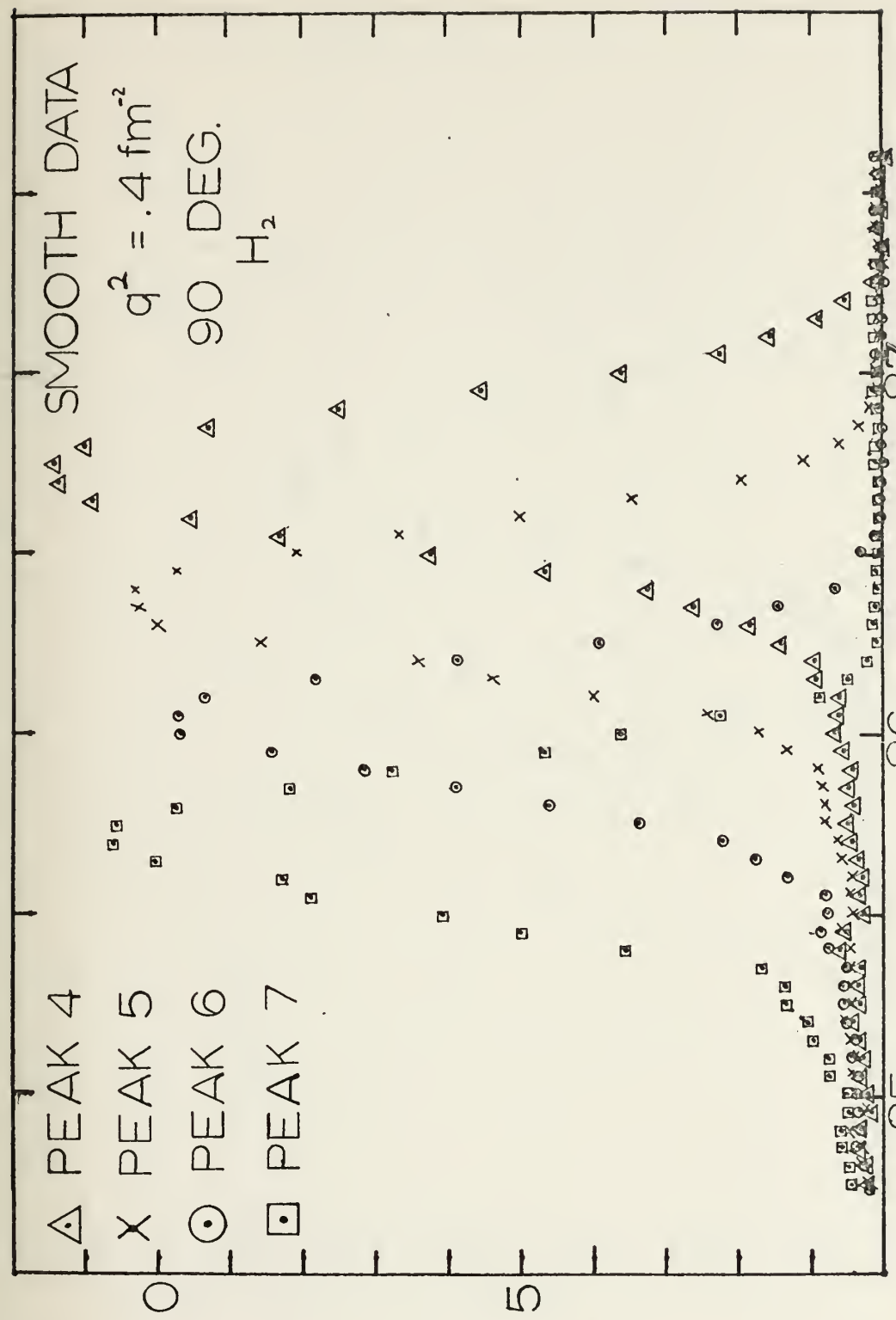
SMOOTH DATA
$q^2 = .4\ fm^{-2}$
90 DEG.
H_2
PEAK 4
PEAK 5
PEAK 6
PEAK 7
10
5
85
86
87
ENERGY (MEV)
COUNTS/COULOMB (10^{-3})

Figure IV-3

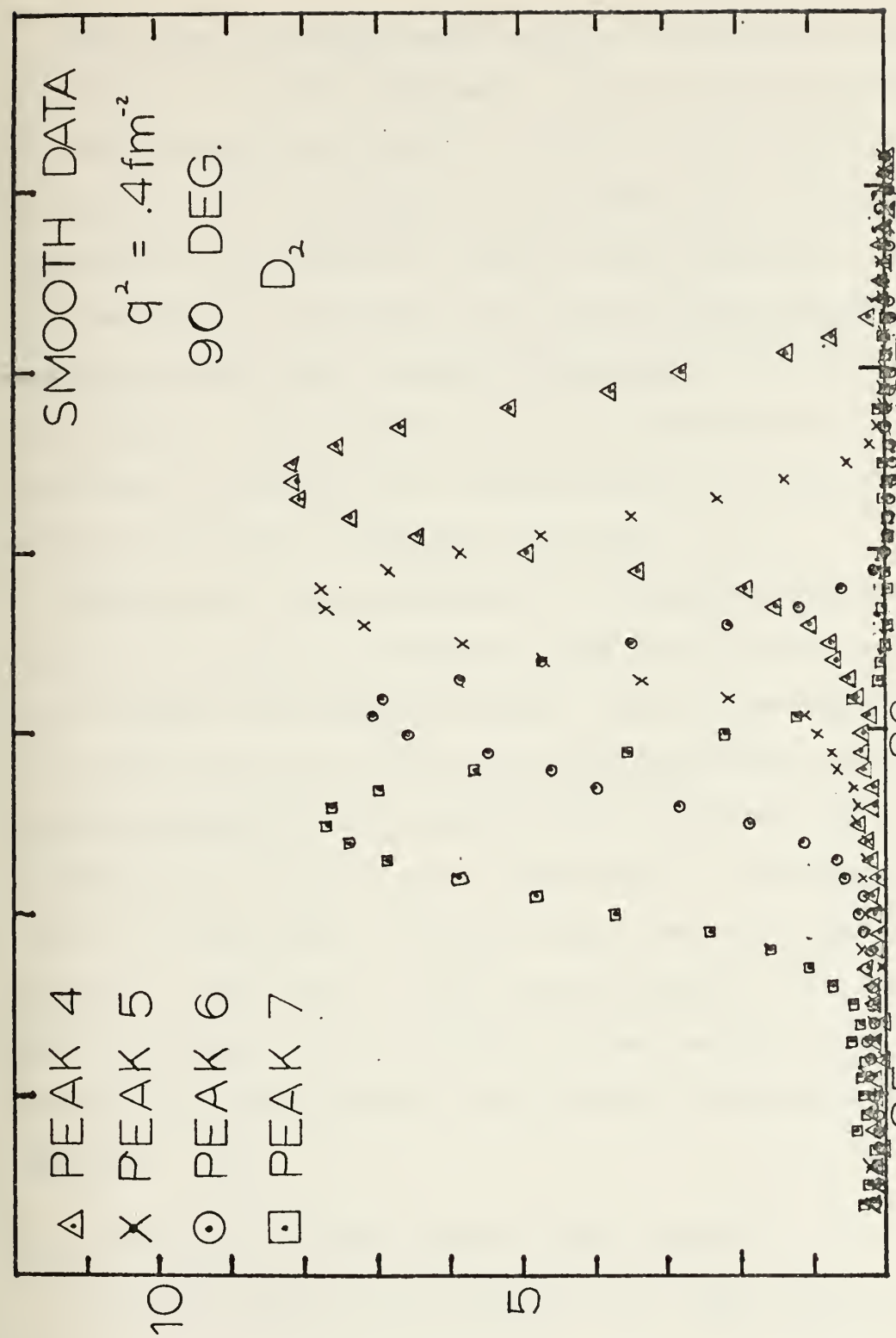
SMOOTH DATA
$q^2 = .4\,fm^{-2}$
90 DEG.
D_2
Δ PEAK 4
× PEAK 5
⊙ PEAK 6
⊡ PEAK 7
10
5
85
86
87
ENERGY (MEV)
COUNTS / COULOMB (10^{-3})

Figure IV-4

The total radiation and ionization corrections, the gas density, the SEM efficiency and the background counts for each channel were typed on computer cards and were used as input data to BERHFORM and TRADFORM along with the appropriate data decks for hydrogen and deuterium. These programs then recalculated the elastic cross section and the statistical error in that cross section for each channel considered. The calculation of the cross section is discussed in Section IV-B, and the method for calculating statistical error is derived in Section IV-D.

Through the use of BERHFORM and TRADFORM, four cross sections (one for each channel) were obtained for each of the hydrogen and deuterium peaks. These cross sections were then put in the form of a ratio (deuterium cross section divided by the hydrogen cross section),and a weighted mean ratio, R_m, was calculated. The electric form factor of the neutron, G_{E_n}, for each run was determined using R_m. The values of the proton electric form factors and the proton and deuteron Mott cross sections and magnetic corrections were obtained from programs TOPROTON and TOPDEUTR [5].

B. CALCULATION OF THE ELASTIC CROSS SECTION

The experimental cross section for each channel is

$$\sigma_{exp} = \frac{N_{sc}\ K_s\ K_b\ K_i}{N_{in}\ N_t\ \Delta\Omega}\ cm^2\ ster^{-1}\ , \qquad \text{(IV-2)}$$

where N_{sc} is the number of scattered electrons counted in a particular channel,

N_{in} is the number of incident electrons,

N_t is the number of target atoms per cm^2,

$\Delta\Omega$ is the solid angle defined by the spectrometer slits,

K_s, K_b, and K_i are radiation and ionization corrections (see Section IV-C),

N_t is given by

$$N_t = \frac{\rho t N_o}{A} , \qquad \text{(IV-3)}$$

where ρ is the density of the target (g/cm^2),

t is the target thickness (cm),

N_o is Avogadro's number, and

A is the atomic weight of the target gas.

N_{in} is determined by

$$N_{in} = \frac{Q}{e} = \frac{CV}{e\,\varepsilon_{sem}} , \qquad \text{(IV-4)}$$

where Q is the total charge of incident electrons,

e is the electron charge (1.60210×10^{-19} coulombs),

V is the voltage of the integrator in volts,

C is the capacitance of the integrator in farads,

ε_{sem} is the SEM efficiency (about 5.8%).

In this experiment a ratio of cross sections is measured, so that several of the parameters of Equations IV-2 and IV-3 which are not absolutely determined, i.e., solid angle and target thickness, cancel with a subsequent elimination of systematic errors.

N_{sc} is the total number of scattered electrons,

$$N_{sc} = \frac{\text{Area under scattering peak (in counts - MeV)}}{\delta E}, \qquad \text{(IV-5)}$$

where E is the energy width of an individual detector.

In order to obtain N_{sc}, the number of counts in a particular channel must be integrated over the energy range of interest.

$$N_{sc} = \sum_{i=1}^{n-1} \frac{1}{2} [N_i + N_{i+1}] (E_i - E_{i+1}) \Big/ 0.0034877\, E_i, \qquad \text{(IV-6)}$$

where N_i is the number of counts in the channel for the i^{th} spectrometer setting, and E_i is the energy of the i^{th} spectrometer setting.

Combining Equations IV-3, IV-4 and IV-6 in Equation IV-2, the experimental cross section may be written as

$$\sigma_{exp} = \frac{\left\{ \sum_{i=1}^{n-1} \frac{1}{2} [N_i + N_{i+1}] (E_i - E_{i+1}) \frac{1}{0.0003487 7 E_i (1.0 + 0.0039 (n-5))} \right\} K_s K_b K_i}{\left(\frac{CV}{e \epsilon_{sem}} \right) \left(\frac{\rho t N_o}{A} \right) \Delta\Omega}, \qquad \text{(IV-7)}$$

where the expression

$$E_{in} = E_i \ (1.0 + 0.0039 \ (n-5)) \qquad \text{(IV-8)}$$

expresses the electron energy seen in counter n in terms of the spectrometer dial setting E_i. Note that counter 5 sees the electron energy read from the spectrometer control dial.

Count rate corrections were applied to N_i by using a linear correction empirically determined from a thick target

experiment. The empirical correction is

$$N_i(\text{count rate corrected}) = \frac{N_i \text{ (recorded)}}{1.0 - 0.00097\ N_i/t_i} ,$$

where N_i/t_i is the average count rate. Background was determined by averaging the counts for each peak above the start of the elastic peak. Charge integration normalization was done as given in Equation IV-1.

C_i is defined as the counts in the i^{th} channel, corrected for background (B), count rate and charge integration normalization.

$$C_i = \frac{N_i \frac{V_{ref}}{V_{act}}}{1 - 0.00097\ N_i/t} - B . \qquad \text{(IV-9)}$$

The final expression for the cross section in terms of defined quantities is

$$\sigma_{exp} = \frac{\frac{1}{2} \sum_{i=1}^{n-1} (C_i + C_{i+1}) \frac{(E_i - E_{i+1})\ K_s K_b K_i}{0.0034877\ (E_{in}/E_i)}}{\left(\frac{CV}{e\varepsilon_{sem}}\right)\left(\frac{\rho t\ N_o}{A}\right)\Delta\Omega} , \qquad \text{(IV-10)}$$

where $\Delta\Omega$ is the solid angle and has a value of 1.831×10^{-3} steradians.

C. RADIATION CORRECTION CALCULATIONS

Both the proton and the deuteron cross section were derived with the assumption of one virtual photon exchange. This process is represented in Figure IV-5. For the deuteron the assumption of the impulse approximation is also made, as

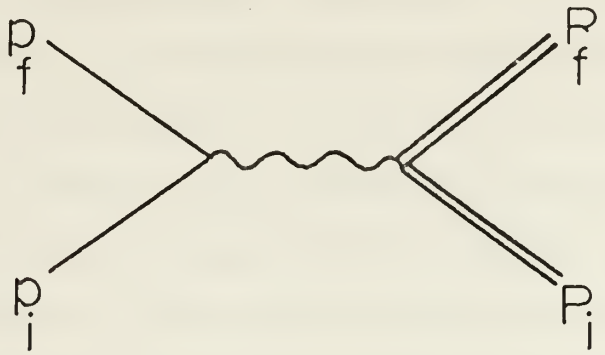

Feynman Diagram of
Rosenbluth Calculation

Figure IV-5

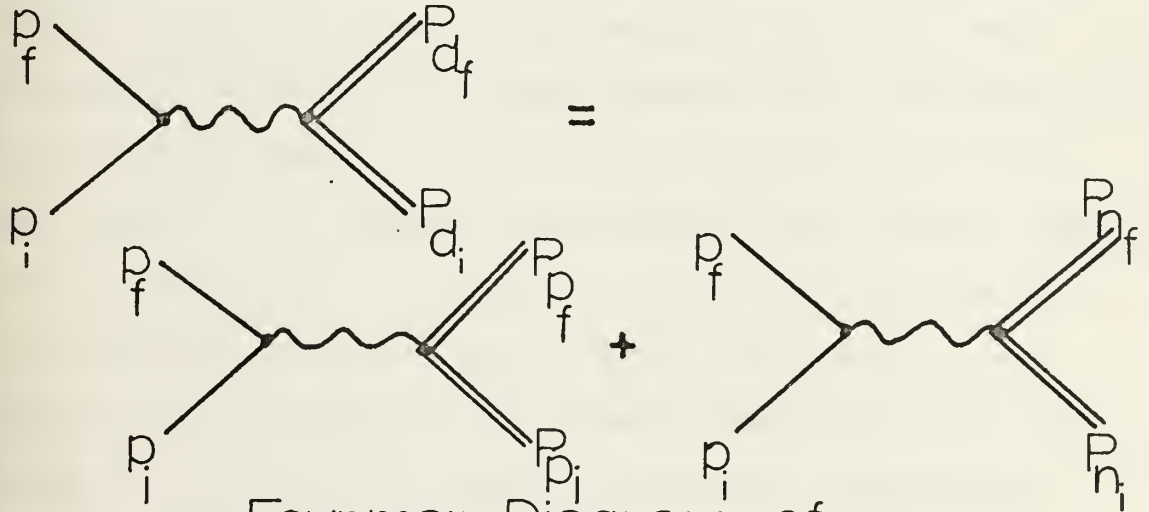

Feynman Diagram of
Impulse Approximation

Figure IV-6

represented in Figure IV-6. However, in the actual scattering process, more processes than those illustrated in the two figures occur. The experimenter must correct for several competing processes in order to be able to compare experiment and theory. These competing processes are

1. The emission of real photons and the reabsorption of virtual photons in the field of the scattering nucleus. The correction to the cross section for this process was first derived by Schwinger [26] and is therefore called the Schwinger Correction.

2. Bremsstrahlung emission in the target before and after the nuclear scattering of interest.

3. Excitation and ionization of material in the target.

In order to obtain the cross section for a nuclear scattering event one would have to continue down to zero energy so as to count all the electrons which have some probability of losing all their energy in the three processes previously discussed. In practice the measurement of the cross section is stopped at some ΔE below the elastic peak, so it is necessary to include a correction to account for the undetected electrons with energy less than $E_f - \Delta E$. Where E_f is the energy of the elastic peak and ΔE is the energy from the elastic peak to the energy corresponding to the last spectrometer setting, usually two to four full widths at half maximum.

C. RADIATION CORRECTION CALCULATIONS

1. Schwinger Correction

The Schwinger correction was generally about 15% in this experiment and is the largest of the three corrections.

The Schwinger correction accounts for processes which occur in addition to the one virtual photon exchange. Schwinger's original work was later improved by Tsai [27] and by Meister and Yennie [28] with the inclusion of the effects of proton recoil. The correction used in this work was evaluated numerically using the expression taken from a review article by Maximon [29].

$$K_s = e^{\delta_s} = \exp\left[\frac{2\alpha}{\pi}\left(\ell n\ \frac{(E_i E_f)^{\frac{1}{2}}}{\Delta E}\right)\left(\ell n\ \frac{q^2}{m^4} - 1\right)\right]\left\{1 + \frac{2\alpha}{\pi}\left[\frac{13}{12}\left(\ell n\ \frac{q^2}{m^2} - 1\right)\right.\right.$$

$$\left.\left. - \frac{1}{4}\ \ell n^2\ \frac{E_i}{E_f} - \frac{17}{36} - \frac{1}{2}\left(\frac{\pi^2}{6} - L_2\left(\cos^2\ \frac{\theta}{2}\right)\right)\right]\right\},$$

where

E_i and E_f are the electron energies before and after scattering,

α is the fine structure constant,

m is the electron mass,

q^2 is the four momentum transfer squared, and

$L_2(x) = -\int_0^x \frac{\ell n\ (1-t)}{t}\, dt$ is the Spence Function.

2. Bremsstrahlung Correction

When an electron passes through material, it will radiate energy through collisions with atomic electrons and nuclei other than the target nucleus of interest. This

energy loss which is referred to as bremsstrahlung has been studied by Bethe and Heitler [30]. The energy loss per distance of material traversed is given by

$$\frac{dE}{dx} = - E X_o ,$$

where X_o is the radiation length, which is the mean distance over which the electron has its energy reduced by a factor of 1/e.

Following Butcher and Messel [33] the radiation length for a multi-element target was calculated using

$$\frac{1}{X_o} = \left(\frac{1}{\sum_i n_i A_i} \right) \left(\sum_i \frac{n_i A_i}{X_o^i} \right) ,$$

where X_o^i is given by

$$X_o^i = \frac{A_i}{4\alpha N_o r_e^2 Z(Z+0.8) \rho_i \ln(183 Z^{-1/3})} ,$$

where N_o is Avogadro's number,

r_e is the classical electron radius,

ρ_i is the density in g/cm^3 of the i^{th} element, and

A_i is in grams/mole of the i^{th} element.

Hofstadter obtained the bremsstrahlung correction factor by integrating the probability function $P(\alpha)$ given by Bethe and Heitler.

$$P(\alpha) = \frac{\alpha^{(t/\ln 2)}}{\Gamma(1+t/\ln 2)} ,$$

where $P(\alpha)$ is the probability that an electron traversing t radiation lengths will have an energy loss less than α

times its initial energy (aside from the ionization loss and the scattering from the nucleus of interest). The bremsstrahlung correction factor is

$$K_b = \exp\left\{ \frac{T}{X_o \ell n 2} \ell n \left(\frac{E}{\Delta E}\right) \right\} ,$$

where T is the thickness of the target (this includes the two steel 1 mil windows as well as the gas) in g/cm^2, and

E is the geometric mean electron energy in the target.

In this experiment the bremsstrahlung correction is about 2%.

3. Ionization Correction

Electrons also lose energy by excitation and ionization in the gas and in the gas target windows. Landau [34] calculated the average energy that a mono-energetic beam would lose, and the spread of the energy distribution of the beam after passing through a thin target. From this distribution it is possible to calculate the fraction of electrons which are not detected because of energy degradation through ionization.

The fraction, $\psi(\Delta E)$, of the beam one does not detect, because of ionization losses is

$$\psi(\Delta E) = \int_o^{E_2} N(E)\, dE \Big/ \int_o^{E_{inc}} n(E)\, dE ,$$

where E_2 is the energy corresponding to the energy of the last spectrometer setting,

E_{inc} is the incident electron energy, and

N(E) is the number of electrons detected at energy E.

Landau [34] derived an approximation for $\psi(\Delta E)$, as have others [35], which is used in this work:

$$\psi(\Delta E) \simeq 1/\omega \ ,$$

where the value of ω as provided by Börsch-Supan [36] is

$$\omega \simeq \lambda\left(1 - \frac{\ell n \lambda + A}{\lambda+1}\right) \ ,$$

where $A \simeq \gamma - 1 = -0.4228...$,

γ is Euler's constant,

$\lambda = \Delta E/\xi - 0.05$

$$\xi = 0.154 \frac{\sum_i \eta_i Z_i}{\sum_i \eta_i A_i} T \text{ MeV, and}$$

T = target thickness in g/cm^2,

η_i is the number of atoms of the i^{th} element per molecule of the target, and Z_i and A_i are the atomic number and atomic weight of the i^{th} element.

The ionization correction is thus given by

$$K_i = [1 - \psi(\Delta E)]^{-1} \ .$$

For both the bremsstrahlung and ionization corrections, the target was treated as a homogeneous molecular compound of steel and either H_2 or D_2, whereas in actuality the target consisted of H_2 or D_2 gas (2 inches thick) at 77°K and 150 psig and two 1 mil steel windows. The molecular formulas used to approximate the target were either Fe H_{26} or Fe D_{26} depending on the gas used.

D. ERROR ANALYSIS

1. Systematic Errors

In this experiment the proton and deuteron cross sections were taken with the same geometry, current, and final electron energies. At most a time delay of twelve hours between the end of the hydrogen and the start of the deuterium run enabled the proton and deuteron data to be taken within a 48 hour time span. Consequently, in the ratio of the deuteron to proton cross sections, many of the systematic errors cancelled; e.g. solid angle, scattering angle, SEM efficiency, target thickness, and absolute spectrometer efficiency.

A systematic error which would not cancel in this ratio experiment is that which arises from impurities in the hydrogen and deuterium gases. The gases used in this experiment were respectively 99.5% deuterium and 99.995% hydrogen, as determined by their supplier [37]. However, the equipment used to establish these purities was able to detect only 0.3% or more contamination of D_2 in H_2 or H_2 in D_2. The data taken in this experiment used the same bottle of deuterium and two different bottles of hydrogen. Consequently, the hydrogen data may have varying amounts of possible contaminants depending on which bottle was used. However, if there were a difference in the contamination of H_2 or D_2, this difference would have caused a non zero intercept of the plot of G_{E_n} versus q^2. This difference was not evident as the value of G_{E_n} $(q^2 = 0)$ is zero to within statistical accuracy for all deuteron models tested.

2. Random Errors

The statistical error is due to the Poisson distribution of the number of electrons scattered for a given number of incident electrons. This error was calculated by a subroutine in the BERHFORM and TRADFORM programs for each individual peak and included the statistical errors made in determining the background subtraction.

If X is the cross section, the following may be written

$$X = (\text{Constant}) \cdot \sum_{k=1}^{M} (N_k - B) ,$$

where N_k is the total counts (count rate and voltage corrected) in the k^{th} spectrometer setting,

B is the average background to be subtracted and is assumed to be the same for each spectrometer setting, and

M is the number of spectrometer settings.

It follows that if $N = N_k$ where N is the total number of counts, then:

$$X - (\text{Constant}) \cdot (N - M \cdot B)$$

The variance of the cross section is

$$\sigma_X^2 = \left(\frac{\partial X}{\partial N}\right)^2 \sigma_N^2 + \left(\frac{\partial X}{\partial B}\right)^2 \sigma_B^2 ,$$

$$\sigma_X^2 = (\text{Constant})^2 \, (N + M^2 \sigma_B^2) ,$$

where σ_B^2 is the variance in the average background, and is equal to B_i. Let $B_T = B_i$ (where B_i is equal to the background at the i^{th} spectrometer setting) and let J be the

number of spectrometer settings above the peak at which background was taken. Since $B = \frac{\sum_{i=1}^{J} B_i}{J}$, then

$$\sigma_B^2 = \frac{1}{J^2} \sum_{i=1}^{J} \sigma_{B_i}^2 = \frac{1}{J^2} \sum_{i=1}^{J} B_i = \frac{1}{J^2} B_T = \frac{B}{J} ,$$

which in turn implies that

$$\sigma_X^2 = (\text{Constant})^2 \ (N + M^2 \frac{B}{J}) ,$$

and the fractional standard deviation of the cross section is

$$\frac{\sigma_X}{X} = \left\{ \frac{N + M^2 \ B/J}{(N-MB)^2} \right\}^{\frac{1}{2}}$$

Besides the statistical (Poisson) counting errors, the random errors in this experiment originate from uncertainties in determining the density of gas in the target, variations in SEM efficiency during a run, energy shifts of the incident beam, leakage currents in the beam current integrators, and small errors in the radiation corrections resulting from errors in determining ΔE.

Uncertainties in determining the density of the gas in the target were caused by the variation of pressure in the target, that is, the pressure dropped while the liquid nitrogen was being pumped and then rose again and stayed steady until the next nitrogen filling. These variations were almost identical in the hydrogen and deuterium runs and were about 0.3% of the measured pressure. The average pressure for each peak in the hydrogen and deuterium runs

was determined separately by either taking the pressure at the start of the nitrogen fill or at the end of the fill depending on which pressure was more constant. If the pressure at the start (completion) of the nitrogen fill was used for hydrogen, then the pressure at the start (completion) of the nitrogen fill was used for deuterium. The errors in the measured cross sections due to the uncertainty in determining the density of the gas in the target varied from run to run, but were always less than 0.1%.

The efficiency of the SEM was measured four times during one data run on each gas, one on each of the four elastic peaks. On each peak, five or more measurements were made. The fractional standard deviation of a single measurement was usually less than 0.2%, giving a standard deviation of the mean of the SEM readings of less than 0.09% for the four readings.

Due to variations in line voltage, the beam energy was not constant, and as a result the scattered energy also changed slightly from time to time throughout a run. Also there was a slight instability in the spectrometer power supply. The instabilities had the effect of shifting the counts from one channel to another on the counting ladder. This variation in the data was most noticeable on the steep slopes of the elastic peaks where a low count in one channel was accompanied by a high count in the adjacent channel. It was found that by closing the energy defining slits more, the variation in the counts due to shifts in energy was

almost negligible. At the same time, it was noticed that the more the energy defining slits were closed the higher the background became. Thus, the ratio of real counts to background counts became less, which in turn increased the errors on the measured cross section. The position for the energy defining slits was adjusted to give the minimum combined contribution to the error in the cross section from the effects of energy shifts and increased background. Even after this was done, in some cases there still existed a need to adjust for obvious energy shifts. This was accomplished by smoothing the data points to the general elastic peak line shape. It is estimated that in the worst case these energy shifts could contribute an uncertainty in the average measured cross section of as much as 0.2%, which the usual error in the measured cross section due to these energy shifts was about 0.1%.

In the circuits used to measure and integrate the beam current there existed slight leakage currents. If these leakage currents were not constant throughout a run, then they would introduce errors. These currents were measured and found to be constant as well as negligible [5]. As a result the only error attributable to these leakage currents existed when the electron beam current varied. The electron current was usually held constant to within 20%. This 20% variation would cause an error in the ratio of the measured cross sections of about 0.02%.

Another source of uncertainty is the inability to determine the exact position of the peak of the elastic spectrum from the plotted data. This uncertainty is usually about 0.01 MeV, and causes an error in the Schwinger, bremsstrahlung, and ionization corrections. The error in the measured cross section due to this ΔE uncertainty for all three radiation corrections was of the order of 0.05%. An uncertainty in the final energy at which one terminates the integration of the elastic spectrum, contributes approximately a 0.03% error to the measurement of the cross section.

A list of all the errors discussed can be found in Table IV-1. Excluding statistical error (since it varies so much from run to run), the average error in the cross section ratio, $S_{\text{Avg. Others}}$, is about 0.24%. The total error of the weighted mean ratio R was then formed from

$$S^2_{\text{total}} = S^2_{\text{stat}} + S^2_{\text{Av. Others}} \qquad \text{(IV-11)}$$

One significant source of error has been reduced since Topping [5] performed his ratio experiment. It was found that if quadrupoles 3 and 4 were used instead of 1, 2, 3 and 4 that the background was effectively 50% lower. The most plausible explanation for this reduction of background is that quadrupoles 1 and 2 defocused the electron beam, causing the beam to hit the beam pipe and thereby increased the background. The data in this experiment was collected with only quadrupoles 3 and 4 on, and as a result, the peak to

TABLE IV-1

RANDOM AND SYSTEMATIC ERRORS IN CROSS SECTION DATA

Errors	Average Values of Errors	
Statistical		0.3%
Gas Density	0.1%	
SEM Efficiency	0.09%	
Energy Shifts	0.1%	
Leakage Currents	0.014%	
E Measurement (Radiation Corrections)	0.05%	
E Measurement (Integration)	0.03%	
Average Error (excluding counting statistics)		0.24%

background ratio of counts was much higher than in the previous work [5].

The uncertainty of G_{E_n} arises from the errors made in measuring the individual cross sections. Let $R = \sigma_d/\sigma_p$ where σ_p and σ_d are the experimental cross sections for the proton and deuteron respectively. Let S_p and S_d be the standard deviation of the proton and deuteron cross sections respectively. G_{E_n} is determined from

$$G_{E_n} = \left[\left(G_{E_d}/G_{E_p}\right)\frac{1}{C_E} - 1.0\right] G_{E_p}(q_d^2) \ , \qquad \text{(IV-12)}$$

and G_{E_d}/G_{E_p} can be determined from

$$\left(G_{E_d}/G_{E_p}\right)^2 = R\,\frac{\sigma^p_{mott}}{\sigma^d_{mott}}\,\frac{K^d_{Mr}}{K^p_M}\left[\frac{G_{E_p}(q^2_p)}{G_{E_p}(q^2_p)}\right]^2 . \qquad \text{(IV-13)}$$

Solving for the standard deviation in R, denoted by S_R, due to the errors in both cross sections, one obtains:

$$S^2_R = R^2\left[\left(\frac{S_d}{\sigma^d}\right)^2 + \left(\frac{S_p}{\sigma^p}\right)^2\right] . \qquad \text{(IV-14)}$$

The standard deviation of the ratio $G_{E_d}.G_{E_p}$, denoted by S_{G_d/G_p}, is obtained from Equation IV-14,

$$S_{G_d/G_p} = \left[\frac{\sigma^p_{mott}}{\sigma^d_{mott}}\,\frac{K^4_{Mr}}{K^4_M}\left(\frac{G_{E_p}(q^2_p)}{G_{E_p}(q^2_p)}\right)^2\right]^{\frac{1}{2}}\frac{S_R}{2\sqrt{R}} . \qquad \text{(IV-15)}$$

From Equation IV-12, one can determine the standard deviation in G_{E_n}, denoted by $S_{G_{E_n}}$, to be:

$$S_{G_{E_n}} = \frac{G_{E_p}(q^2 d)}{C_E}\left(\frac{G_{E_d}}{G_{E_p}}\right)\frac{S_R}{R} . \qquad \text{(IV-16)}$$

In order to combine the results obtained from four different channels in one run, let R_i denote the ratio of cross sections in the i^{th} channel and let S_{R_i} denote the standard deviation of the ratio in the i^{th} channel. It follows that the weighted mean ratio R_m can be calculated from

$$R_m = \frac{\sum_{i=4}^{7}\left(R_i/S^2_{R_i}\right)}{\sum_{i=4}^{7}\left(1/S^2_{R_i}\right)} , \qquad \text{(IV-17)}$$

where the standard deviation of this weighted mean ratio is calculated from

$$S_{R_m} = \left[\frac{1}{\sum_{i=4}^{7} \left(1/S_{R_i}^2 \right)} \right]^{\frac{1}{2}} . \qquad \text{(IV-18)}$$

R_m and S_{R_m} are the experimental values of the ratio and of the standard deviation to that ratio.

V. EXPERIMENTAL RESULTS

A. NEUTRON CHARGE FORM FACTORS

The 21 runs by Topping [5] and the twelve runs by the authors are reported here. Each run consisted of four measurements of R, the ratio of the elastic electron-deuteron cross section to the elastic electron-proton cross section. Of these 132 measurements of R, 9 were not included due to reasons given in Ref. [5].

Table V-1 gives the q^2 transferred to the deuteron, the scattering angle, the experimental ratio R_m, and the standard deviation of R_m determined both for the total error and the statistical (Poisson) error for a given run. Also included are quantities that were determined by calculations discussed in Section II. The ratio of the deuteron electric form factor to the proton electric form factor, derived using relativistic corrections by both Friar and Gross, is also listed in Table V-1.

Tables V-2,3,4 and 5 present the neutron charge form factors obtained using the deuteron models LF1,5, and 15 with the relativistic corrections of Gross and Friar. The deuteron structure factors used are presented in Appendix D. The best estimates of the error in each of these 33 values of G_{E_n} for each LF model and relativistic correction is the error obtained using S_{total} from Equation IV-11. An average G_{E_n} and the associated S_{total} at each q^2 were calculated using Equations V-1 and V-2 respectively.

$$(G_{E_n})_m = \frac{\sum_i \frac{(G_{E_n})_i}{(S^2_{tot})_i}}{\sum_i \frac{1}{(S^2_{tot})_i}} \qquad \text{(V-1)}$$

$$(S_{tot})_m = \left[\sum_i \frac{1}{(S^2_{tot})_i}\right]^{-\frac{1}{2}} \qquad \text{(V-2)}$$

A plot of the average G_{E_n} (with its S_{tot}) versus q^2 is provided for each of three LF models and both relativistic corrections.

All values of G_{E_n} were calculated on a Wang Model 700-C calculator using programs written by the authors. The best estimate of the slope of G_{E_n} versus q^2, $d/dq^2\ G_{E_n}$, was obtained from a linear fit weighted by S_{tot} for all values of G_{E_n}. For comparison purposes the linear fit was also forced through zero for each plot.

The average value of G_{E_n} at each q^2, using Lomon-Feshbach Model #1 is given in Table V-2.

The average value of G_{E_N} at each q^2, using Lomon-Feshbach Model #5 is given in Table V-3.

The average value of G_{E_n} at each q^2, using Lomon-Feshbach Model #15 is given in Table V-4.

The value of G_{E_n} calculated from Lomon-Feshbach Model #15 and its $S_{G_{E_n}}$ for each of the 33 runs is given in Table V-5.

B. ROSENBLUTH PLOT

At $q^2 = 0.4$ fm^{-2} deuteron and hydrogen data were taken at 90° and 120° so that a Rosenbluth plot could be constructed. The theoretical interpretation of the Rosenbluth plot is discussed in Appendix A. Table V-6 gives the experimental data and derived quantities used in the Rosenbluth plot given in Figure V-7. The use of the scaling law is compatible with the data.

C. CHARGE RADIUS OF THE DEUTERON

Using Method II given by Schumacher and Bethe [7], the deuteron structure rms radius was calculated. A more detailed explanation is given in Appendix B. The structure radius of the deuteron for LF1, LF5, and LF15 was provided by Schumacher and Bethe [7] and was used in a plot of the experimental $\left[\frac{d}{dq^2} G_{E_n}\right]_{q^2=0}$ versus $r^2_{E_d}$ (deuteron structure radius). This plot is Figure V-8 and as predicted by Schumacher such a plot gives a straight line for all models with the correct binding energy. The intersection of this line with the value of $\left[\frac{d}{dq^2} G_{E_n}\right]_{q^2=0}$ determined by the very accurate neutron-electron scattering work yields $r^2_{E_d}$. The value for the deuteron structure rms radius was determined from Figure V-8 to be $r_E = 1.9665 \pm 0.0045$.

TABLE V-1

EXPERIMENTAL RATIOS AND RESULTS OF
MODEL INDEPENDENT CALCULATIONS

q_d^2 (fm^{-2})	θ	Exp. Ratio $R = \frac{d}{p}_{exp}$	Std. Dev. of R Total and (stat.)	$\frac{\sigma^p_{mott}}{\sigma^d_{mott}}$	$G_{E_p}(q_p^2)$	$G_{E_p}(q_d^2)$
0.05	60°	0.9654	0.0046 (0.0040)	0.30269 0.31356	0.99400	0.99404
	75°	0.9724	0.0038 (0.0030)	0.16837 0.17578	0.99396	0.99404
0.10	75°	0.9390	0.0042 (0.0035)	0.81525 0.86757	0.98789	0.98815
	75°	0.9331	0.0034 (0.0024)	0.81525 0.86757	0.98789	0.98815
	75°	0.9262	0.0046 (0.0038)	0.81525 0.86757	0.98789	0.98815

q_d^2 (fm^{-2})	θ	$\frac{K^d_{M_r}\text{ (Gross)}}{K^d_{M_r}\text{ (Friar)}}$	K^p_M	(Gross) $\frac{G_{E_d}}{G_{E_p}}$ Total and $\pm$(stat) Error	(Friar) $\frac{G_{E_d}}{G_{E_p}}$ Total and $\pm$(stat) Error
0.05	60°	1.00001 1.00001	0.99338	0.9685±0.0023 (0.0020)	0.9685±0.0023 (0.0020)
	75°	0.99997 0.99996	0.99114	0.9693±0.0019 (0.0015)	0.9693±0.0019 (0.0015)
0.10	75°	0.99993 0.99992	0.98230	0.9475±0.0021 (0.0018)	0.9475±0.0021 (0.0018)
	75°	0.99993 0.99992	0.98230	0.9445±0.0017 (0.0012)	0.9445±0.0017 (0.0012)
	75°	0.99993 0.99992	0.98230	0.9410±0.0023 (0.0019)	0.9410±0.0023 (0.0019)

TABLE V-1 (Continued)

q_d^2 (fm^{-2})	θ	Exp. Ratio $R = \frac{\sigma^d_{exp}}{\sigma^p_{exp}}$	Std. Dev. of R Total and (Stat.)	$\frac{\sigma^p_{mott}}{\sigma^d_{mott}}$	$G_{E_p}(q_p^2)$	$G_{E_p}(q_d^2)$
0.10	75°	0.9221	0.0040 (0.0031)	0.81525 0.86757	0.98789	0.98815
0.20	60°	0.8204	0.0051 (0.0045)	0.70815 0.76120	0.97595	0.97653
	60°		0.0076 (0.0072	0.70815 0.76120	0.97595	0.97653
	75°	0.8402	0.0049 (0.0042)	0.39041 0.42650	0.97582	0.97653
	90°	0.8323	0.0049 (0.0042)	0.22434 0.24871	0.97569	0.97653
	90°	0.8365	0.0052 (0.0046)	0.22434 0.24871	0.97569	0.97653

q_d^2 (fm^{-2})	θ	$\frac{K^d_{M_r}\text{ (Gross)}}{K^d_{M_r}\text{ (Friar)}}$	K^p_M	(Gross) $\frac{G_{E_d}}{G_{E_p}}$ ± Total and (Stat) Error	(Friar) $\frac{G_{E_d}}{G_{E_p}}$ ± Total and (Stat) Error
0.10	75°	0.99993 0.99992	0.98230	0.9389±0.0020 (0.0016)	0.9389±0.0020 (0.0016)
0.20	60°	1.00001 1.00001	0.97359	0.8848±0.0028 (0.0024)	0.8848±0.0028 (0.0024)
	60°	1.00001 1.00001	0.97359	0.8887±0.0041 (0.0039)	0.8887±0.0041 (0.0039)
	75°	0.99985 0.99985	0.96493	0.8921±0.0026 (0.0022)	0.8921±0.0026 (0.0022)
	90°	0.99896 0.99896	0.95129	0.8871±0.0026 (0.0022)	0.8871±0.0026 (0.0022)
	90°	0.99896 0.99896	0.95129	0.8893±0.0028 (0.0024)	0.8893±0.0028 (0.0024)

TABLE V-1 (Continued)

q_d^2 (fm^{-2})	θ	Exp. Ratio $R = \frac{\sigma^d_{exp}}{\sigma^p_{exp}}$	Std. Dev. of R Total and (Stat.)	$\frac{\sigma^p_{mott}}{\sigma^d_{mott}}$	$G_{E_p}(q_p^2)$	$G_{E_p}(q_d^2)$
0.20	120°	0.8068	0.0118 (0.0106)	0.72058 0.81829	0.97555	0.97653
	120°	0.8280	0.0102 (0.0099)	0.71893 0.81637	0.97550	0.97653
	120°	0.8057	0.0082 (0.0079)	0.71893 0.81637	0.97550	0.97653
0.25	75°	0.7987	0.0056 (0.0051)	0.30690 0.33890	0.96982	0.97082
0.30	75°	0.6973	0.0049 (0.0043)	0.27183 0.28073	0.96625	0.96516
	90°	0.7718	0.0057 (0.0052)	0.14386 0.16338	0.96365	0.96516

q_d^2 (fm^{-2})	θ	$\frac{K^d_{M_r}\text{ (Gross)}}{K^d_{M_r}\text{ (Friar)}}$	K^p_M	(Gross) $\frac{G_{E_d}}{G_{E_p}} \pm$ Total and (Stat) Error	(Friar) $\frac{G_{E_d}}{G_{E_p}} \pm$ Total and (Stat) Error
0.20	120°	0.99466 0.99466	0.89020	0.8901±0.0065 (0.0058)	0.8901±0.0065 (0.0058)
	120°	0.99465 0.99464	0.88999	0.9018±0.0055 (0.0054)	0.9018±0.0055 (0.0054)
	120°	0.99465 0.99464	0.88999	0.8896±0.0045 (0.0044)	0.8895±0.0045 (0.0044)
0.25	75°	0.99982 0.99981	0.95641	0.8687±0.0030 (0.0028)	0.8687±0.0030 (0.0028)
0.30	75°	0.99978 0.99977	0.95135	0.8426±0.0030 (0.0026)	0.8426±0.0030 (0.0026)
	90°	0.99845 0.99844	0.92817	0.8538±0.0031 (0.0029)	0.8538±0.0031 (0.0029)

TABLE V-1 (Continued)

q_d^2 (fm^{-2})	θ	Exp. Ratio $R = \frac{\sigma^d_{exp}}{\sigma^p_{exp}}$	Std. Dev. of R Total and (Stat.)	$\frac{\sigma^p_{mott}}{\sigma^d_{mott}}$	$G_{E_p}(q_p^2)$	$G_{E_p}(q_d^2)$
0.30	90°	0.7529	0.0060 (0.0055)	0.14386 0.16338	0.96365	0.96516
	90°	0.7558	0.0070 (0.0066)	0.14386 0.16338	0.96365	0.96516
0.35	90°	0.7192	0.0054 (0.0048)	0.12122 0.13916	0.95767	0.95955
	90°	0.6596	0.0056 (0.0051	0.13341 0.13916	0.96112	0.95955
0.40	90°	0.6815	0.0056 (0.0050	1.04376 1.210236	0.951718	0.95400
	90°	0.6829	0.0058 (0.0053)	1.04376 1.21024	0.95172	0.95400

q_d^2 (fm^{-2})	θ	$\frac{K^d_{M_r}\text{ (Gross)}}{K^d_{M_r}\text{ (Friar)}}$	K^p_M	(Gross) $\frac{G_{E_d}}{G_{E_p}}$ ± Total and (Stat) Error	(Friar) $\frac{G_{E_d}}{G_{E_p}}$ ± Total and (Stat) Error
0.30	90°	0.99845 0.99844	0.92817	0.8433±0.0034 (0.0031)	0.8433±0.0034 (0.0031)
	90°	0.99845 0.99844	0.92817	0.8449±0.0039 (0.0037)	0.8449±0.0039 (0.0037)
0.35	90°	0.99819 0.99818	0.91695	0.8242±0.0031 (0.0027)	0.8242±0.0031 (0.0027)
	90°	0.99819 0.99818	0.92340	0.8281±0.0035 (0.0032)	0.8281±0.0035 (0.0032)
0.40	90°	0.997933 0.997918	0.905924	0.8027±0.0033 (0.0030)	0.8027±0.0033 (0.0030)
	90°	0.997933 0.997918	0.905924	0.8036±0.0034 (0.0031)	0.8036±0.0034 (0.0031)

TABLE V-1 (Continued)

q_d^2 (fm^{-2})	θ	Exp. Ratio $R = \frac{\sigma^d_{exp}}{\sigma^p_{exp}}$	Std. Dev. of R Total and (Stat.)	$\frac{\sigma^p_{mott}}{\sigma^d_{mott}}$	$G_{E_p}(q_p^2)$	$G_{E_p}(q_d^2)$
0.40	120°	0.6430	0.0062 (0.0057)	0.32879 0.39489	0.95117	0.95400
	120°	0.6266	0.0061 (0.0056)	0.32879 0.39489	0.95117	0.95400
	120°	0.6300	0.0062 (0.0057)	0.32879 0.39489	0.95117	0.95400
0.477	90°	0.6324	0.0061 (0.0056)	0.85522 1.00679	0.94262	0.94550
	90°	0.6389	0.0051 (0.0045)	0.85522 1.00679	0.94262	0.94550
	90°	0.6330	0.0060 (0.0055)	0.85522 1.00679	0.94022	0.94500

q_d^2 (fm^{-2})	θ	$\frac{K^d_{M_r}\text{ (Gross)}}{K^d_{M_r}\text{ (Friar)}}$	K^p_M	(Gross) $\frac{G_{E_d}}{G_{E_p}}$ ± Total and (Stat) Error	(Friar) $\frac{G_{E_d}}{G_{E_p}}$ ± Total and (Stat) Error
0.40	120°	0.98938 0.98936	0.79894	0.8118±0.0039 (0.0036)	0.8118±0.0039 (0.0036)
	120°	0.98938 0.98936	0.79894	0.8014±0.0039 (0.0036)	0.8014±0.0039 (0.0036)
	120°	0.98938 0.98936	0.79894	0.8036±0.0039 (0.0036)	0.8036±0.0039 (0.0036)
0.477	90°	0.99754 0.99752	0.88935	0.7739±0.0037	0.7739±0.0037 (0.0034)
	90°	0.99754 0.99752	0.88935	0.7778±0.0031 (0.0027)	0.7778±0.0031 (0.0027)
	90°	0.99754	0.88935	0.7742±0.0037 (0.0034)	0.7742±0.0037 (0.0034)

TABLE V-1 (Continued)

q_d^2 (fm^{-2})	θ	Exp. Ratio $R = \frac{\sigma^d_{exp}}{\sigma^p_{exp}}$	Std. Dev. of R Total and (Stat.)	$\frac{\sigma^p_{mott}}{\sigma^d_{mott}}$	$G_{E_p}(q_p^2)$	$G_{E_p}(q_d^2)$
0.50	105°	0.6033	0.0057 (0.0052)	0.46122 0.55662	0.93952	0.94307
	105°	0.6042	0.0057 (0.0052)	0.46122 0.55662	0.93952	0.94307
	105°	0.6044	0.0058 (0.0053)	0.46122 0.55662	0.93952	0.94307
	105°	0.6015	0.0060 (0.0055)	0.46122 0.55662	0.93952	0.94307

q_d^2 (fm^{-2})	θ	$\frac{K^d_{M_r}\text{ (Gross)}}{K^d_{M_r}\text{ (Friar)}}$	K^p_M	(Gross) $\frac{G_{E_d}}{G_{E_p}}$ ± Total and (Stat) Error	(Friar) $\frac{G_{E_d}}{G_{E_p}}$ ± Total and (Stat) Error
0.50	105°	0.99368 0.99366	0.83642	0.7677±0.0036 (0.0033)	0.7677±0.0036 (0.0033)
	105°	0.99368 0.99366	0.83642	0.7683±0.0036 (0.0033)	0.7683±0.0036 (0.0033)
	105°	0.99368 0.99366	0.83642	0.7685±0.0037 (0.0034)	0.7685±0.0037 (0.0034)
	105°	0.99368 0.99366	0.83642	0.7666±0.0038 (0.0035)	0.7666±0.0038 (0.0035)

TABLE V-2

AVERAGE G_{E_n} AT EACH q^2 USING LOMON-FESHBACH MODEL #1

q^2 (fm^{-2})	Gross' Relativistic Correction		Friar's Relativistic Correction	
	G_{E_n}	$S_{G_{E_n}}$	G_{E_n}	$S_{G_{E_n}}$
0.05	0.0002	0.0015	0.0002	0.0015
0.10	0.0037	0.0011	0.0037	0.0011
0.20	0.0027	0.0013	0.0027	0.0013
0.25	0.0070	0.0034	0.0069	0.0034
0.30	0.0076	0.0019	0.0075	0.0019
0.35	0.0093	0.0027	0.0092	0.0027
0.40	0.0084	0.0020	0.0081	0.0020
0.477	0.0098	0.0025	0.0095	0.0025
0.50	0.0106	0.0023	0.0102	0.0023

A linear fit to the data in Table V-2 gives:

$G_{E_n} = (0.0003 \pm 0.0010) + (0.0208 \pm 0.0040)q^2$ for Gross' correction and

$G_{E_n} = (0.0004 \pm 0.0010) + (0.0200 \pm 0.0040)q^2$ for Friar's correction.

A linear fit of the same data forced through zero gives:

$G_{E_n}(q^2) = (0.0218 \pm 0.0022)q^2$ for Gross' correction and

$G_{E_n}(q^2) = (0.0213 \pm 0.0022)q^2$ for Friar's correction.

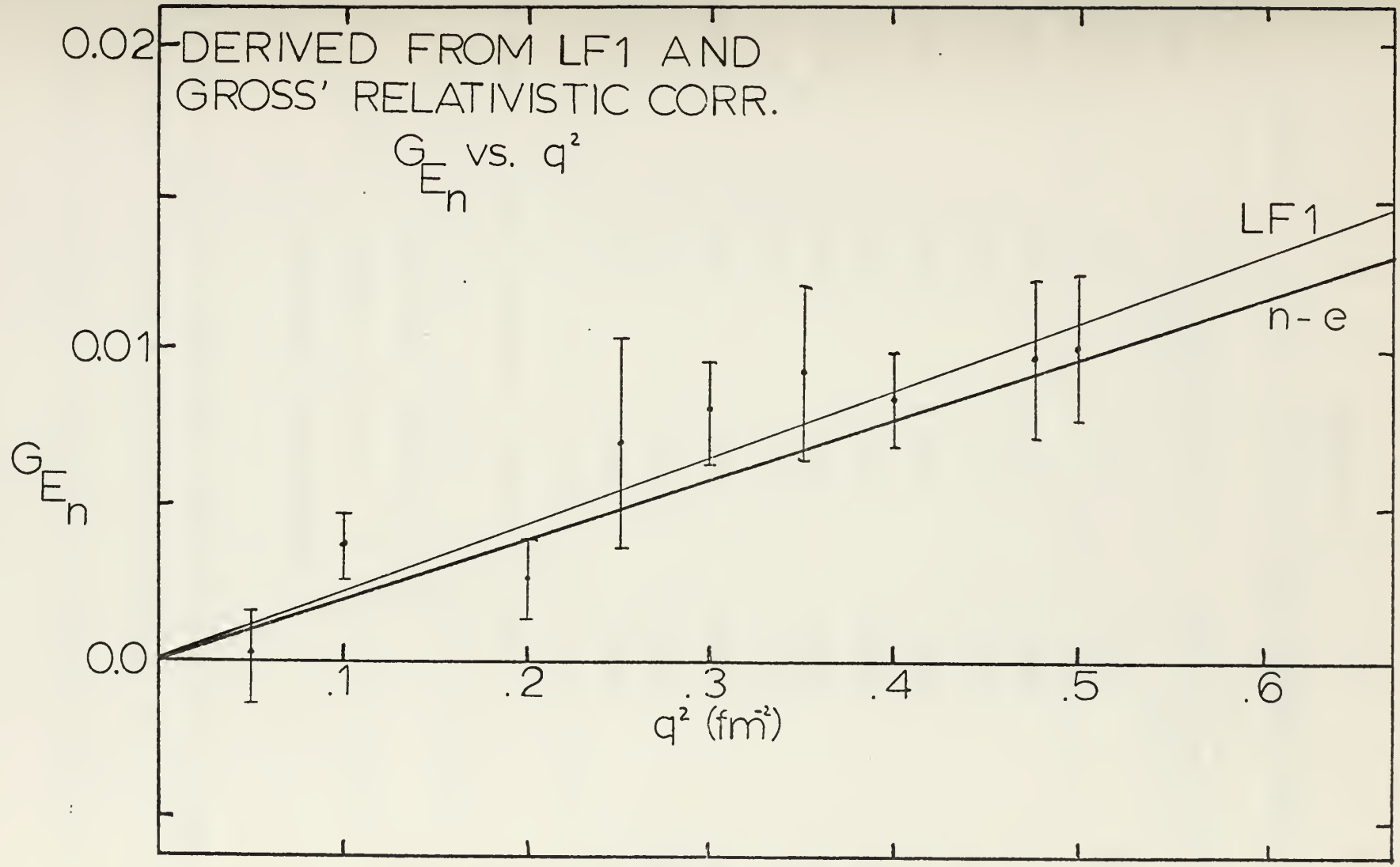
DERIVED FROM LF1 AND
GROSS' RELATIVISTIC CORR.
G_{E_n} vs. q^2
LF1
n-e
0.02
0.01
0.0
G_{E_n}
.1
.2
.3
.4
.5
.6
q^2 (fm^{-2})

Figure V-1

TABLE V-3

AVERAGE G_{E_n} AT EACH q^2 USING LOMON-FESHBACH MODEL #5

q^2 (fm^{-2})	Gross' Relativistic Correction		Friar's Relativistic Correction	
	G_{E_n}	$S_{G_{E_n}}$	G_{E_n}	$S_{G_{E_n}}$
0.05	0.0002	0.0015	0.0002	0.0015
0.10	0.0037	0.0011	0.0037	0.0011
0.20	0.0028	0.0013	0.0027	0.0013
0.25	0.0070	0.0034	0.0069	0.0034
0.30	0.0076	0.0019	0.0075	0.0019
0.35	0.0094	0.0027	0.0092	0.0027
0.40	0.0084	0.0020	0.0082	0.0020
0.477	0.0099	0.0025	0.0096	0.0025
0.50	0.0107	0.0023	0.0103	0.0023

A linear fit to the data in Table V-3 gives:

$$G_{E_n}(q^2) = (0.0003 \pm 0.0010) + (0.0210 \pm 0.0040)q^2$$

for Gross' correction and

$$G_{E_n}(q^2) = (0.0004 \pm 0.0010) + (0.0202 \pm 0.0040)q^2$$

for Friar's correction.

A linear fit of the same data forced through zero gives:

$G_{E_n}(q^2) = (0.0220 \pm 0.0022)q^2$ for Gross' correction and

$G_{E_n}(q^2) = (0.0214 \pm 0.0022)q^2$ for Friar's correction.

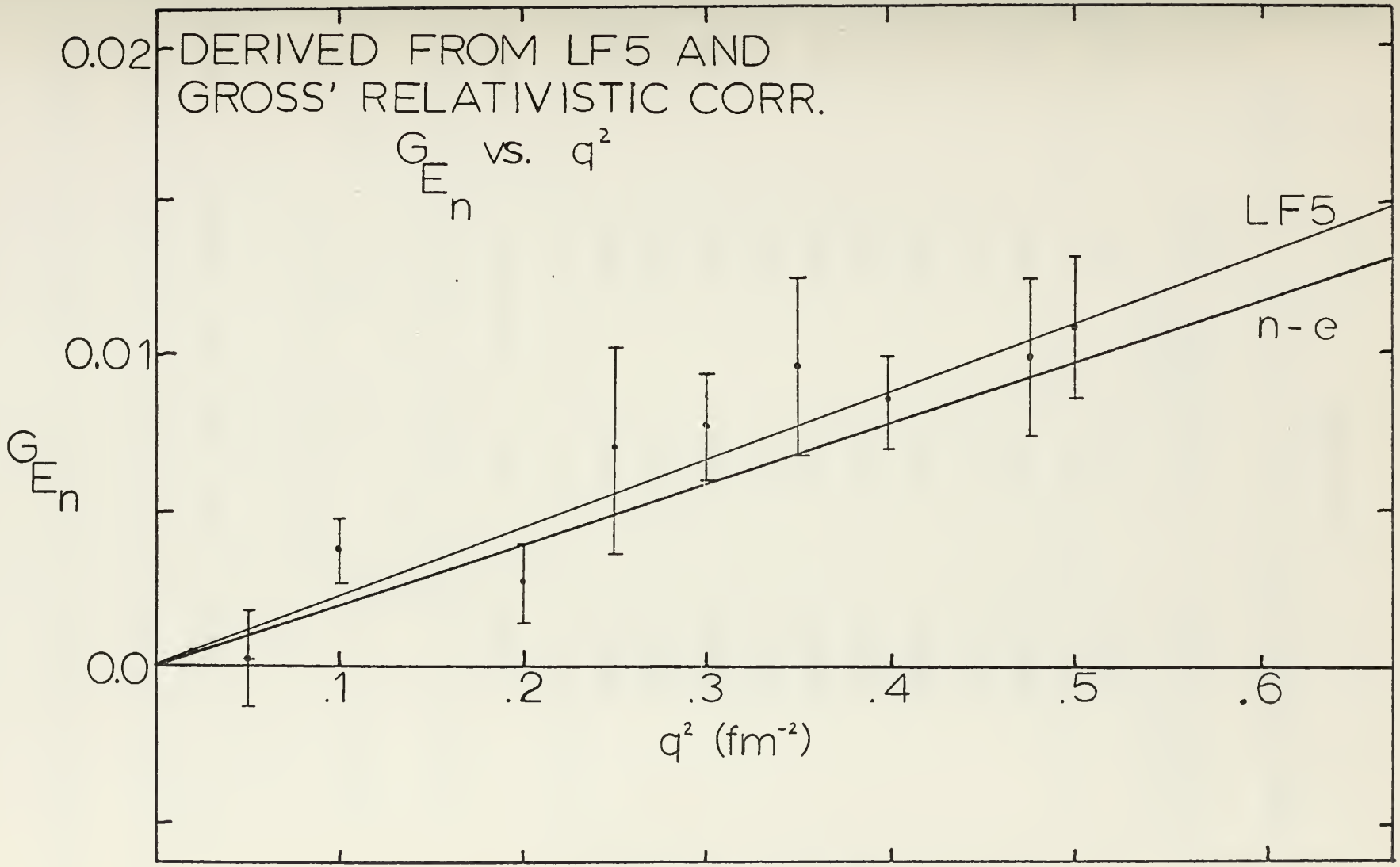
DERIVED FROM LF5 AND
GROSS' RELATIVISTIC CORR.
G_{E_n} vs. q^2
LF5
n-e
0.02
0.01
0.0
G_{E_n}
.1
.2
.3
.4
.5
.6
q^2 (fm^{-2})

Figure V-2

TABLE V-4

AVERAGE G_{E_n} AT EACH q^2 USING LOMON-FESHBACH MODEL #15

q^2 (fm^{-2})	Gross' Relativistic Correction		Friar's Relativistic Correction	
	G_{E_n}	$S_{G_{E_n}}$	G_{E_n}	$S_{G_{E_n}}$
0.05	0.0000	0.0015	-0.0000	0.0015
0.10	0.0033	0.0011	0.0033	0.0011
0.20	0.0020	0.0013	0.0020	0.0013
0.25	0.0061	0.0034	0.0060	0.0034
0.30	0.0066	0.0019	0.0066	0.0019
0.35	0.0082	0.0027	0.0080	0.0027
0.40	0.0070	0.0020	0.0068	0.0020
0.477	0.0083	0.0025	0.0080	0.0025
0.50	0.0090	0.0023	0.0086	0.0023

A linear fit to the data in Table V-4 gives:

$$G_{E_n}(q^2) = (0.0002 \pm 0.0010) + (0.0177 \pm 0.0040)q^2$$

for Gross' correction and

$$G_{E_n}(q^2) = (0.0003 \pm 0.0010) + (0.0170 \pm 0.0040)q^2$$

for Friar's correction.

A linear fit of the same data forced through zero gives:

$G_{E_n}(q^2) = (0.0185 \pm 0.0022)q^2$ for Gross' correction and

$G_{E_n}(q^2) = (0.0180) \pm 0.0022)q^2$ for Friar's correction.

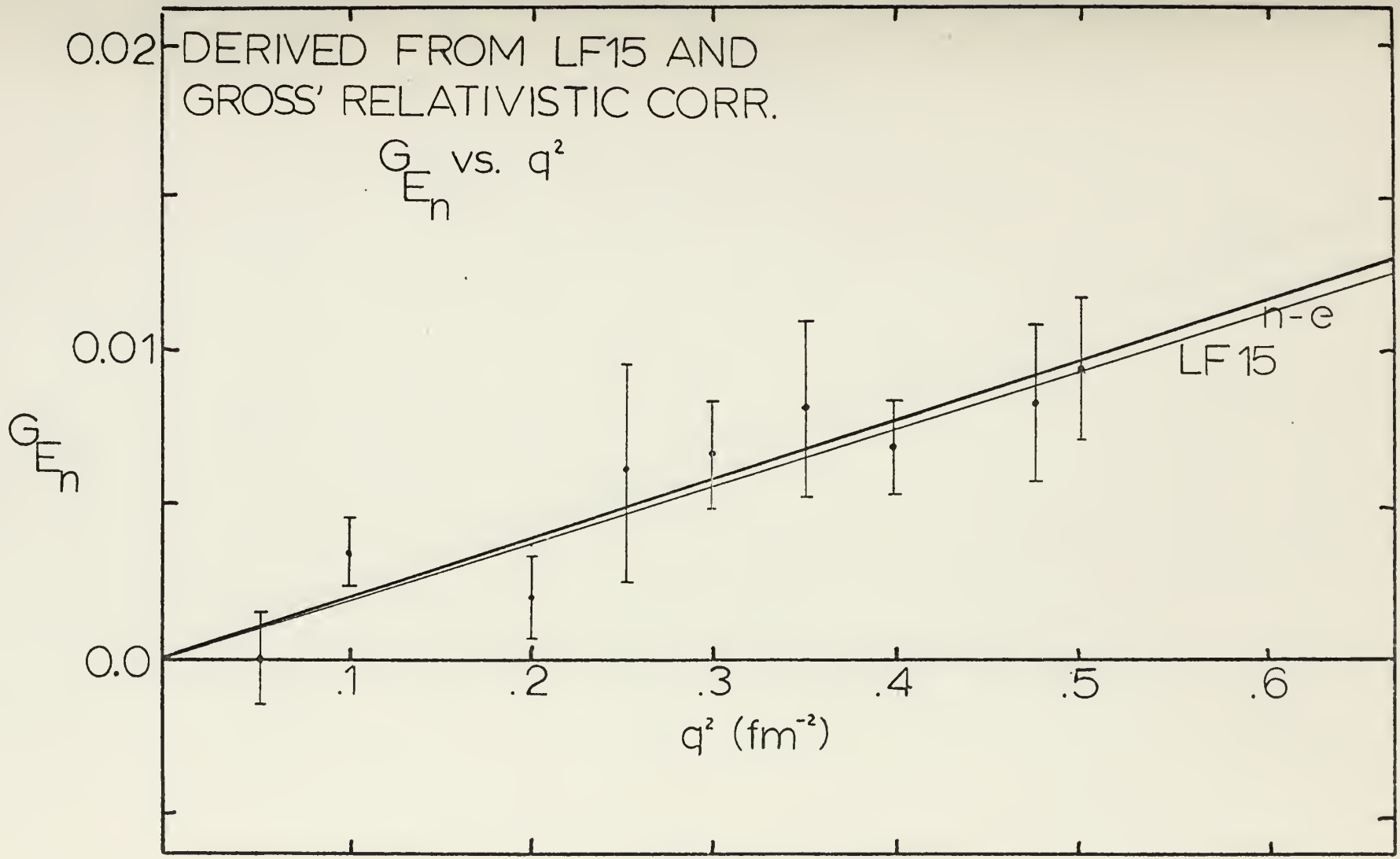
DERIVED FROM LF15 AND
GROSS' RELATIVISTIC CORR.
G_{E_n} vs. q^2
0.02
0.01
0.0
G_{E_n}
n-e
LF 15
.1
.2
.3
.4
.5
.6
q^2 (fm^{-2})

Figure V-3

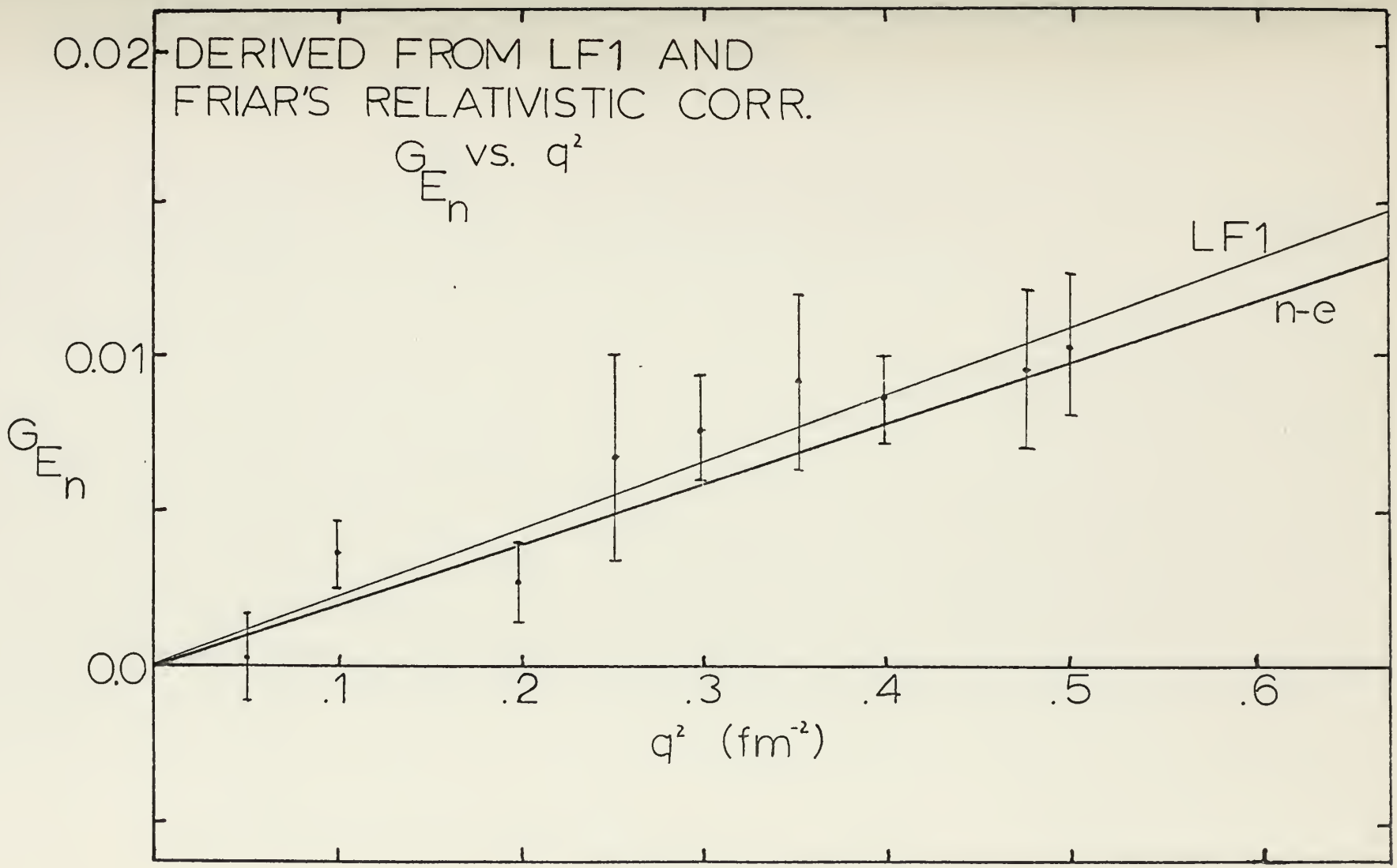
DERIVED FROM LF1 AND
FRIAR'S RELATIVISTIC CORR.
G_{E_n} vs. q^2
LF1
n-e
0.02
0.01
0.0
G_{E_n}
.1
.2
.3
.4
.5
.6
q^2 (fm^{-2})

Figure V-4

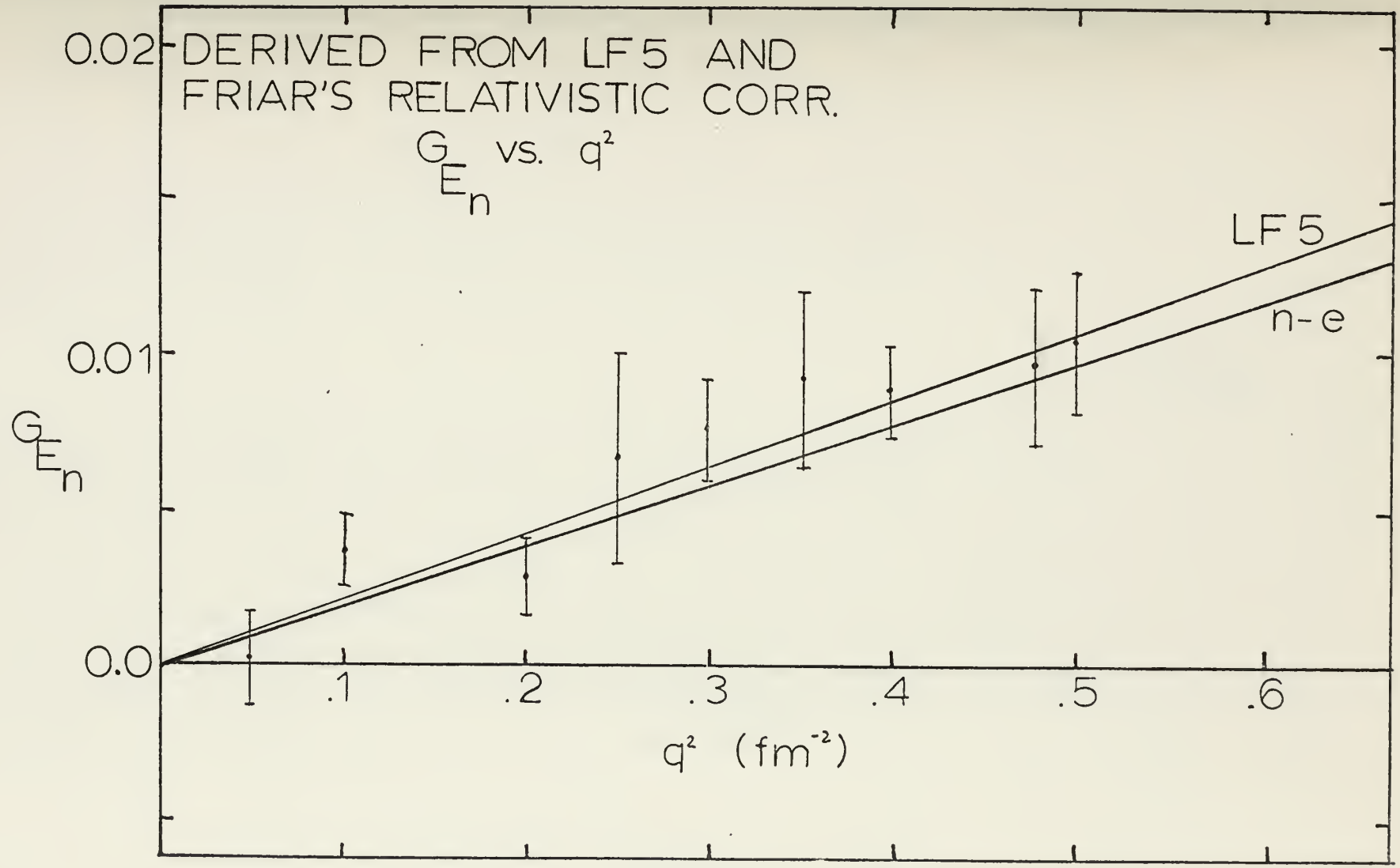
DERIVED FROM LF5 AND
FRIAR'S RELATIVISTIC CORR.
G_{E_n} vs. q^2
LF5
n-e
0.02
0.01
0.0
G_{E_n}
.1
.2
.3
.4
.5
.6
q^2 (fm^{-2})

Figure V-5

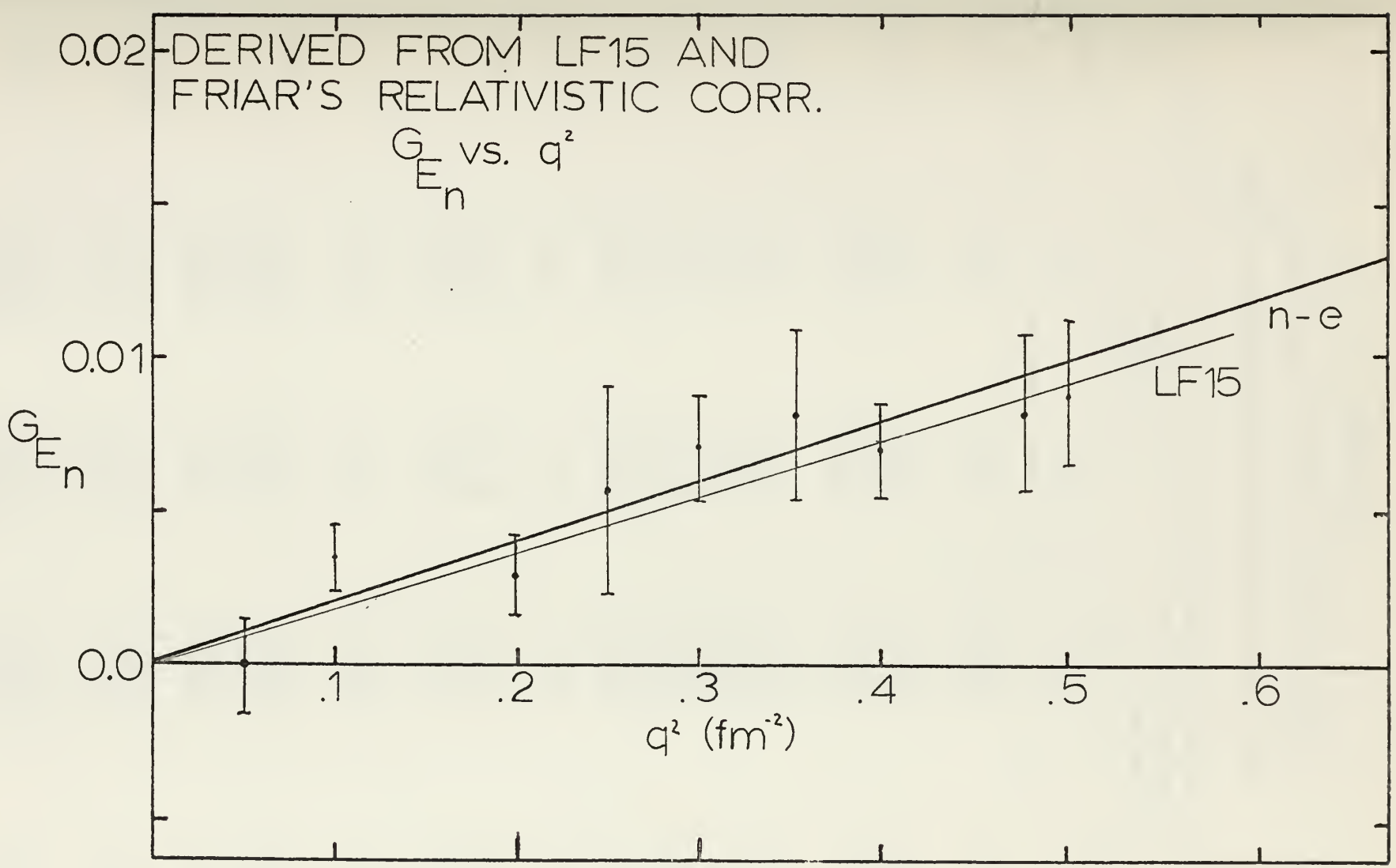
DERIVED FROM LF15 AND
FRIAR'S RELATIVISTIC CORR.
G_{E_n} vs. q^2
0.02
0.01
0.0
G_{E_n}
n-e
LF15
.1
.2
.3
.4
.5
.6
q^2 (fm^{-2})

Figure V-6

TABLE V-5

G_{E_n} AND S_{tot} FOR EACH OF THE 30 RUNS
CALCULATED FROM LOMON-FESHBACH MODEL #15

q^2 (fm^{-2})	Gross' Relativistic Correction		Friar's Relativistic Correction	
	G_{E_n}	$S_{G_{E_n}}$	G_{E_n}	$S_{G_{E_n}}$
0.05	0.0003	0.0019	0.0003	0.0019
	-0.0005	0.0024	-0.0005	0.0024
0.10	0.0078	0.0022	0.0078	0.0022
	0.0010	0.0025	0.0010	0.0025
	0.0047	0.0018	0.0047	0.0018
	-0.0012	0.0021	-0.0012	0.0021
0.20	-0.0027	0.0030	-0.0028	0.0030
	0.0015	0.0045	0.0014	0.0045
	0.0052	0.0029	0.0052	0.0029
	-0.0002	0.0029	-0.0003	0.0029
	0.0021	0.0030	0.0021	0.0030
	0.0030	0.0072	0.0030	0.0072
	0.0159	0.0061	0.0158	0.0061
	0.0025	0.0050	0.0024	0.0050
0.25	0.0061	0.0034	0.0060	0.0034
0.30	0.0153	0.0036	0.0151	0.0036
	0.0032	0.0039	0.0030	0.0039
	0.0050	0.0045	0.0049	0.0045
	0.0024	0.0034	0.0023	0.0034
0.35	0.0061	0.0036	0.0060	0.0036
	0.0108	0.0041	0.0106	0.0041
0.40	0.0050	0.0039	0.0048	0.0039
	0.0060	0.0041	0.0058	0.0041
	0.0159	0.0047	0.0157	0.0047
	0.0034	0.0046	0.0032	0.0046
	0.0060	0.0047	0.0058	0.0047
0.477	0.0061	0.0046	0.0058	0.0046
	0.0110	0.0038	0.0107	0.0038
	0.0066	0.0045	0.0063	0.0045
0.50	0.0089	0.0045	0.0086	0.0045
	0.0096	0.0045	0.0092	0.0045
	0.0098	0.0046	0.0095	0.0046
	0.0074	0.0047	0.0071	0.0047

TABLE V-6

$G_d^2(q^2)$, DEUTERON FORM FACTOR SQUARED AT $q^2 = 0.4$ fm^{-2}

Scattering Angle (degrees)	$1+2(1+\eta)\tan^2\frac{\theta}{2}$	$R \pm S_R$(total)	σ^p deVries $(\times 10^{29})$cm^2	$\sigma_M^d(\theta)$ $(\times 10^{29})$cm^2	$G_d^2 \pm S_{G_s}^2$
90	2.0043	0.6815 ± 0.0056	1.10265	1.21024	0.6209 ± 0.0051
90	2.0043	0.6829 ± 0.0058	1.10265	1.21024	0.6222 ± 0.0053
120	7.0262	0.6430 ± 0.0062	0.39362	0.39489	0.6454 ± 0.0062
120	7.0262	0.6265 ± 0.0061	0.39362	0.39489	0.6266 ± 0.0061
120	7.0262	0.6300 ± 0.0062	0.39362	0.39489	0.6323 ± 0.0062

A linear fit to the data in Table V-6 showed that

$$G_d^2(0.4) = (0.6163 \pm 0.0053) + (0.0026 \pm 0.0010)\ [1 + 2(1+\eta)\tan^2\frac{\theta}{2}]$$

If the first 120° run, which is well outside the error bars of the others is omitted,

$$G_d^2(0.4) = (0.6184 \pm 0.0054) + (0.0016 \pm 0.0011)\ [1 + 2(1+\eta)\tan^2\frac{\theta}{2}]$$

The slope from the scaling law is 0.00097.

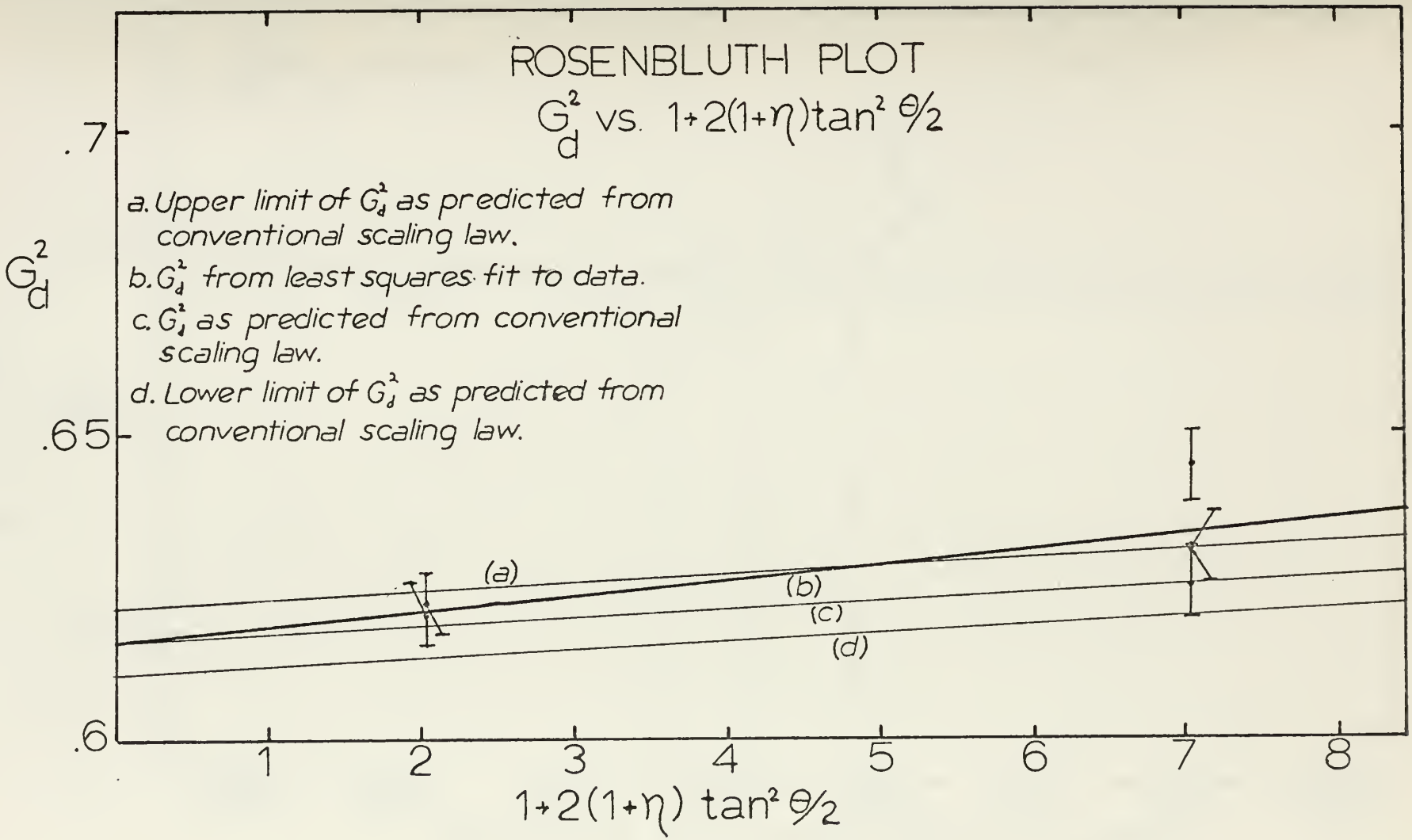
ROSENBLUTH PLOT
G_d^2 vs. $1+2(1+\eta)\tan^2\theta/2$
a. Upper limit of G_d^2 as predicted from conventional scaling law.
b. G_d^2 from least squares fit to data.
c. G_d^2 as predicted from conventional scaling law.
d. Lower limit of G_d^2 as predicted from conventional scaling law.
G_d^2
.7
.65
.6
(a)
(b)
(c)
(d)
1
2
3
4
5
6
7
8
$1+2(1+\eta)\tan^2\theta/2$

Figure V-7

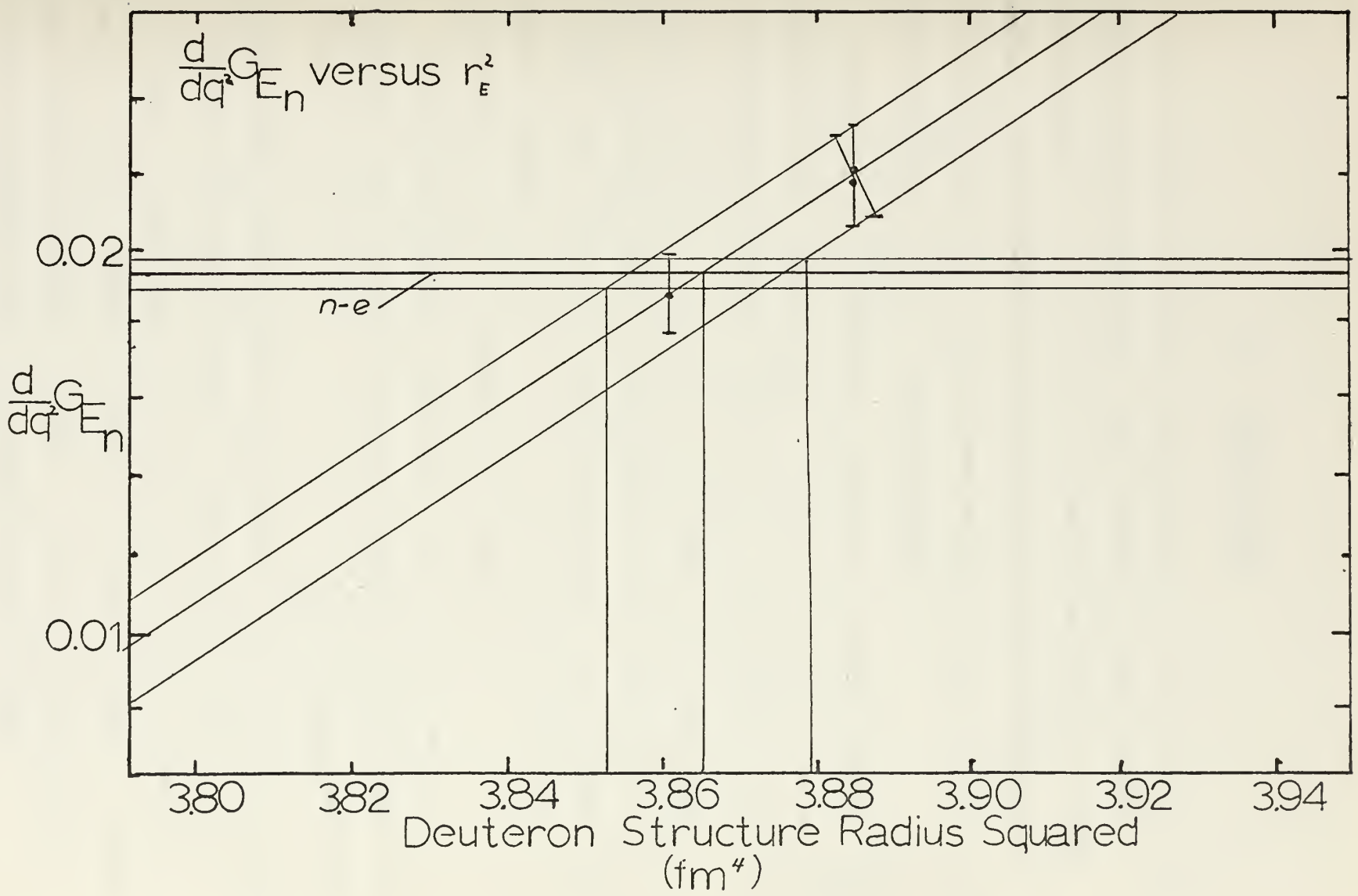
$\frac{d}{dq^2}G_{E_n}$ versus r_E^2
0.02
0.01
n-e
$\frac{d}{dq^2}G_{E_n}$
3.80
3.82
3.84
3.86
3.88
3.90
3.92
3.94
Deuteron Structure Radius Squared
(fm⁴)

Figure V-8

VI. CONCLUSIONS

As a result of the 123 measurements of the ratio of the elastic electron-deuteron cross section to the elastic electron-proton cross section, nine values of G_{E_n} at different values of q^2 were determined for each deuteron wave function considered. From these values of G_{E_n} and q^2, a value of $\left[\frac{d}{dq^2} G_{E_n}\right]_{q^2=0}$ was determined.

Relativistic corrections proposed by both Friar [8] and Gross [6] were investigated. It was found that, for a given deuteron wave function, $\left(\frac{d}{dq^2} G_{E_n}\right)_{q^2=0}$ was smaller using the Friar correction. Although this pattern was consistent, it was also found that the difference in the two slopes was always well within one standard deviation. No attempt was made to select one form of the relativistic correction as best because the difference was so small.

All wave functions considered (LF1, 5, 15) were in agreement with the very accurate thermal neutron slope of $(0.0193 \pm .0004)$ fm^2. The values of $\left[\frac{d}{dq^2} G_{E_n}\right]_{q^2=0}$ obtained using Gross' relativistic corrections were: for LF1 $(0.0218 \pm \pm 0.0022)$, for LF5 (0.0220 ± 0.0022) and for LF15 (0.0185 ± 0.0022). The values obtained using Friar's corrections were: for LF1 (0.0213 ± 0.0022), for LF5 (0.0214 ± 0.0022), and for LF15 (0.0180 ± 0.0022). LF15 was found to be in closest agreement with the thermal neutron slope.

A value for the structure radius of the deuteron was also obtained from this data. This value was determined by comparing the slopes given by each wave function. The structure radius was determined to be $r_E = (1.9665 \pm 0.0045)$fm.

A Rosenbluth plot was made at $q^2 = 0.4$ fm^{-2}. The results of this plot are discussed in Appendix A and show agreement with the use of the conventional deuteron scaling law.

If this experiment were to be repeated or extended it is recommended that data at higher q^2 be taken in order to determine more accurately the coefficient of the q^4 term in the expansion of G_{E_n}. In Appendix C a coefficient for the q^4 term was taken from work done at DESY [38] and it was found that at $q^2 = 0.5$ fm^{-2} this term decreases G_{E_n} by about 10%. The effect on the slope of the G_{E_n} curve is also shown to be about a 7% increase.

APPENDIX A

THE ROSENBLUTH PLOT

Based on the one photon exchange, the cross section for electron-proton scattering was derived by Rosenbluth [10]. Using the same assumption (one photon exchange) Jankus [14] calculated the deuteron cross section. Jankus' result is given in Equation II-7 and is reproduced below

$$\frac{d\sigma^d}{d\Omega} = \left(\frac{d\sigma^d}{d\Omega}\right)_{mott}\left\{G_{E_d}^2 + \frac{8}{9}\eta^2 G_{Q_d}^2 + \frac{2}{3}\eta G_{M_d}^2\left[1 + 2(1+\eta)\tan^2\frac{\theta}{2}\right]\right\},$$

where G_d^2 can be written as

$$G_d^2 = \left\{G_{E_d}^2(q^2) + \frac{8}{9}\eta^2 G_{Q_d}^2 + \frac{2}{3}\eta G_{M_d}^2\left[1 + 2(1+\eta)\tan^2\frac{\theta}{2}\right]\right\}.$$

Since the deuteron cross section can be measured at different scattering angles while at the same four momentum transfer, one can see that a plot of G_d^2 versus $(1 + 2(1+\eta)\tan^2\frac{\theta}{2})$ should give a straight line with $\frac{2}{3}\eta G_{M_d}^2$ as the slope and $G_{E_d}^2 + \frac{8}{9}\eta^2 G_{Q_d}^2$ as the intercept. By plotting the deuteron total form factor G_d^2 versus $[1+2(1+\eta)\tan^2\frac{\theta}{2}]$, the adequacy of the conventional scaling law can be tested. Such a plot has been made for $q^2 = 0.4$ fm^{-2} and it can be found in Section V.

One cannot use Equation II-7 directly since it contains the absolute cross section of the deuteron. However the deuteron cross section can be obtained by using the hydrogen

cross section along with the deVries b' fit. The deVries b' cit [19] is used because it is the best fit to the absolute proton cross section. It is used as a normalization factor with the experimental cross section obtained from the data. That is,

$$\left(\frac{d\sigma^p}{d\Omega}\right)_{deVries} = N \left(\frac{d\sigma^p}{d\Omega}\right)_{exp} .$$

Therefore,

$$N = \left\{ \left(\frac{d\sigma^p}{d\Omega}\right)_{deVries} \Big/ \left(\frac{d\sigma^p}{d\Omega}\right)_{exp} \right\} .$$

N is a normalization factor for a given experiment at a given angle and energy. Since both the proton cross section and the deuteron cross section were measured under the same experimental conditions, the deuteron cross section is

$$\left(\frac{d\sigma^d}{d\Omega}\right) = N \left(\frac{d\sigma^d}{d\Omega}\right)_{exp} .$$

This implies that

$$\left(\frac{d\sigma^d}{d\Omega}\right) = \left\{ \left(\frac{d\sigma^p}{d\Omega}\right)_{deVries} \Big/ \left(\frac{d\sigma^p}{d\Omega}\right)_{exp} \right\} \left(\frac{d\sigma^d}{d\Omega}\right)_{exp} .$$

Now putting this in terms of the experimental ratio R, where R is given by

$$R = \left(\frac{d\sigma^d}{d\Omega}\right)_{exp} \Big/ \left(\frac{d\sigma^p}{d\Omega}\right)_{exp} ,$$

one obtains

$$\left(\frac{d\sigma^d}{d\Omega}\right) = R \left(\frac{d\sigma^p}{d\Omega}\right)_{deVries} ,$$

and recalling that

$$\left(\frac{d\sigma^d}{d\Omega}\right) = \left(\frac{d\sigma^d}{d\Omega}\right)_{mott} G_d^2 ,$$

one gets the final expression for G_d^2 as

$$G_d^2 = \left\{ \left(\frac{d\sigma^p}{d\Omega}\right)_{deVries} \Big/ \left(\frac{d\sigma^d}{d\Omega}\right)_{mott} \right\} R_m ,$$

where $\left(\frac{d\sigma^p}{d\Omega}\right)_{deVries}$ was calculated from the BERROTON program and $\left(\frac{d\sigma^d}{d\Omega}\right)_{mott}$ was calculated from the BERDEUTR program and the ratio R_m is the weighted mean ratio given by Equation IV-17.

The statistical error in G_d^2 was calculated using the following equation;

$$S_{G_d^2} = \frac{\left(\frac{d\sigma^p}{d\Omega}\right)_{deVries}}{\left(\frac{d\sigma^d}{d\Omega}\right)_{mott}} S_{R_m} ,$$

where S_{R_m} is given by Equation IV-18.

APPENDIX B

RMS STRUCTURE RADIUS OF DEUTERON

By substituting the deuteron charge distribution for the neutron charge distribution, it can be shown that an expression similar to Equation II-15 for the deuteron is applicable.

$$G_d(q^2) = G_d(0) - \frac{\langle r_d^2 \rangle}{6} q^2 + \frac{\langle r_d^4 \rangle}{120} q^4 + \ldots \qquad \text{(B-1)}$$

where r_d^2 is the mean square radius of the deuteron charge distribution. In principle, the deuteron form factor could be fit to this polynomial form and the slope of $G_d(q^2)$ versus q^2 in the limit as q^2 approaches zero would be $-\frac{\langle r_d^2 \rangle}{6}$. However, for the deuteron, the coefficient of the q^4 term is not well determined and the choice of $\langle r_d^4 \rangle$ greatly affects the value of $\langle r_d^2 \rangle$. In order to determine $\langle r_d^4 \rangle$, data at higher momentum transfer is necessary and its determination requires knowledge of the coefficient of the q^6 term.

Fortunately, Schumacher and Bethe [7] have suggested a procedure to avoid this problem. The method consists of using the experimental data and the function $C_E(q^2)$ associated with a deuteron wave function to calculate A in the expansion

$$G_{E_n}(q^2) = A_q^2 + B_q^4 \,. \qquad \text{(B-2)}$$

If the deuteron structure factor C_E is also expanded for small q^2, the expansion is:

$$C_E(q^2) = 1 - \frac{1}{6} \langle r_E^2 \rangle q^2 + \frac{1}{120} \langle r_E^4 \rangle q^4 + \ldots, \quad \text{(B-3)}$$

where $\langle r_E^2 \rangle$ may be defined as the mean square radius of the deuteron structure factor.

Schumacher and Bethe observed that if the same data set is used to calculate A from various C_E functions, which have different values of $\langle r_E^2 \rangle$, the plot of A as a function of $\langle r_E^2 \rangle$ forms a straight line, if one uses only C_E functions corresponding to deuteron models which have the correct binding energy. Then, if one requires that A have the value deduced from the neutron-electron scattering experiment, the value of $\langle r_E^2 \rangle$ may be determined, as shown in Figure V-8. The error in $\langle r_E^2 \rangle$ is fixed by the intersection of the projection of the errors of A, and the slope obtained using models considered in this experiment. The value of $\langle r_E^2 \rangle$ is given in Section V.

Finally, one may note that the mean square charge radius, $\langle r_d^2 \rangle$ may be found from:

$$\langle r_d^2 \rangle = \langle r_E^2 \rangle + \langle r_p^2 \rangle - 6A \ .$$

APPENDIX C

q^4 DEPENDENCE OF G_{E_n}

In Chapter IV, the slope of G_{E_n} was determined assuming a linear fit of G_{E_n} versus q^2, but there was some evidence that the inclusion of a quadratic term may be more appropriate. Therefore, a fit with both linear and quadratic terms was made to the data, but it was discovered that such a fit produced a quadratic coefficient of little confidence.

Since the value of the coefficient for the linear term is not strongly dependent on the value of the quadratic coefficient, for this data, a value for the quadratic coefficient was assumed using the work of Galster et al. [39]. Galster et al. obtained the value $B = -0.0036$ fm^4 for the quadratic coefficient and this value was used in application to this work's data. A recalculation for the quadratic coefficient of the analytic expression,

$$G_{E_n} = Aq^2 + Bq^4 ,$$

shows that the quadratic term contributes 5% to G_{E_n} at $q^2 = 0.35$ fm^{-2} and 10% at $q^2 = 0.5$ fm^{-2}. With the assumed quadratic coefficient, the slope of G_{E_n} increased by 7% from that obtained without the inclusion of the quadratic term. Also, the deuteron structure radius is decreased by 0.15%. Note that the changes in the slope and the deuteron

structure radius are within the statistical accuracy of the value previously reported in Chapter IV. A comparative table of values utilized in the linear and quadratic fits can be found in Tables C-1 and C-2.

TABLE C-1

COMPARISON OF G_{E_n} AND $G_{E_n} - Bq^4$

q^2 (fm^{-2})	LF5		LF15	
	G_{E_n}	$G_{E_n} - Bq^4$	G_{E_n}	$G_{E_n} - Bq^4$
0.05	0.0002	0.0002	0.0000	0.0000
0.10	0.0037	0.0037	0.0033	0.0033
0.20	0.0028	0.0029	0.0020	0.0021
0.25	0.0070	0.0072	0.0061	0.0063
0.30	0.0076	0.0079	0.0066	0.0069
0.35	0.0094	0.0098	0.0082	0.0086
0.40	0.0084	0.0089	0.0070	0.0076
0.477	0.0099	0.0107	0.0083	0.0091
0.50	0.0107	0.0116	0.0090	0.0098

For LF1 assuming $B = -0.0036$ fm^4
$A = 0.0232 \pm 0.0022$

For LF5 assuming $B = -0.0036$ fm^4
$A = 0.0232 \pm 0.0022$

For LF15 assuming $B = -0.0036$ fm^4
$A = 0.0198 \pm 0.0023$

TABLE C-2

COMPARISON OF THE DEUTERON STRUCTURE RADIUS OBTAINED FROM THE LINEAR AND QUADRATIC FITS TO G_{E_n}, ASSUMING GROSS RELATIVISTIC CORRECTION

	$G_{E_n} = Aq^2$	$G_{E_n} = Aq^2 + bq^4$
$\langle r_E^2 \rangle$	3.867 ± 0.018	3.858 ± 0.018
$r_{E_{rms}}$	1.9665 ± 0.0045	1.9642 ± 0.0045

APPENDIX D

COMPARISON OF GROSS' AND FRIAR'S RELATIVISTIC CORRECTION

Both the Gross and Friar relativistic corrections multiply the right hand side of Equation II-7. The Gross relativistic correction factor is given by:

$$\left(1 - \frac{q^2}{8M_p^2}\right)^2 = 1 - \frac{q^2}{4M_p^2} + \frac{q^4}{64\ M_p^4}\ , \qquad \text{(D-1)}$$

and Friar's correction factor is

$$\left(1 + \frac{q^2}{4M_p^2}\right)^{-1}\ .$$

Expanding Friar's correction in a binomial series to second order in $\frac{q^2}{4M_p^2}$, the following is obtained:

$$\left(1 + \frac{q^2}{4M_p^2}\right)^{-1} = 1 - \frac{q^2}{4M_p^2} + \frac{q^4}{16M_p^4}\ , \qquad \text{(D-2)}$$

The difference between the two relativistic correction factors is approximately given by the difference between Equation D-2 and D-1. If this difference is given the symbol Δ then,

$$\Delta \approx \frac{q^4}{M_p^4}\left[\frac{1}{16} - \frac{1}{64}\right] = \frac{3}{64}\ \frac{q^4}{M_p^4}\ . \qquad \text{(D-3)}$$

The difference is seen to increase with increasing q^2. At $q^2 = 0.5\ fm^{-2}$, which is the highest q^2 investigated, Δ

is 2.3×10^{-5} with Friar's correction always being greater. Since the corrections are both about 0.997 for $q^2 = 0.5$ fm^{-2}, then the difference in these two corrections is about two parts in 10^5. Table D-1 gives a comparison of both corrections for all q^2's investigated

Friar [8] also shows that C_E, the electric structure factor of the deuteron, should not be evaluated at q^2 but at an effective $q^{2'}$ given by

$$q^{2'} = \frac{q^2}{1 + \frac{q^2}{4M_d^2}} . \qquad \text{(D-4)}$$

This also creates a very small change as seen in Tables D-2, D-3 and D-4. Friar's first relativistic correction opposes the tendency of the use of the effective momentum transfer, so the net difference between the use of the Friar and Gross corrections is smaller than four parts in 10^4. Also included in these tables is a comparison of the slope of G_{E_n} versus q^2 using each correction. Again the difference is seen to be negligible for this experiment.

TABLE D-1

COMPARISON OF RELATIVISTIC CORRECTION FACTORS

q^2 fm^{-2}	Friar's Relativistic Correction	Gross' Relativistic Correction	$1 - \frac{\text{Friar}}{\text{Gross}}$
0.05	.999972	.999972	-.000000
0.10	.999447	.999448	-.000001
0.20	.998894	.998896	-.000002
0.25	.998618	.998621	-.000003
0.30	.998341	.998345	-.000004
0.35	.998065	.998070	-.000006
0.40	.997788	.997796	-.000007
0.477	.997360	.997370	-.000010
0.50	.997235	.997247	-.000011

TABLE D-2

COMPARISON OF $C_E(q^2)$ AND $C_E(q^{2'})$ FOR LF1

q^2	$C_E(q^2)$	q^2	$C_E(q^{2'})$	$1 - \frac{C_E(q^{2'})}{C_E(q^2)}$
0.05	.96882	0.0500	.96882	-.00000
0.10	.93967	0.1000	.93969	-.00001
0.20	.88668	0.1999	.88673	-.00006
0.25	.86247	0.2498	.86256	-.00009
0.30	.83961	0.2998	.83972	-.00013
0.35	.81796	0.3497	.81810	-.00017
0.40	.79742	0.3996	.79760	-.00023
0.477	.76766	0.4765	.76790	-.00030
0.50	.75929	0.4997	.75955	-.00034

Slope of G_{E_n} versus q^2 using Gross' correction is 0.0218 ± 0.0022.

Slope of G_{E_n} versus q^2 using Friar's correction is 0.0213 ± 0.0022.

TABLE D-3

COMPARISON OF $C_E(q^2)$ and $C_E(q^{2'})$ FOR LF5

q^2	$C_E(q^2)$	q^2	$C_E(q^{2'})$	$1 - \frac{C_E(q^{2'})}{C_E(q^2)}$
0.05	.96881	0.0500	.96881	-.00000
0.10	.93966	0.100	.93968	-.00002
0.20	.88665	0.1999	.88670	-.00006
0.25	.86244	0.2498	.86252	-.00010
0.30	.83956	0.2998	.83968	-.00014
0.35	.81790	0.3497	.81805	-.00018
0.40	.79735	0.3996	.79754	-.00023
0.477	.76759	0.4765	.76782	-.00031
0.50	.75921	0.4997	.75947	-.00034

Slope of G_{E_n} versus q^2 using Gross' correction is
0.0220 ± 0.0022.

Slope of G_{E_n} versus q^2 using Friar's correction is
0.0214 ± 0.0022.

TABLE D-4

COMPARISON OF $C_E(q^2)$ AND $C_E(q^{2'})$ FOR LF15

q^2	$C_E(q^2)$	q^2	$C_E(q^{2'})$	$1 - \frac{C_E(q^{2'})}{C_E(q^2)}$
0.05	.96900	0.0500	.96900	-.00000
0.10	.94002	0.1000	.94003	-.00002
0.20	.88731	0.1999	.88737	-.00006
0.25	.86324	0.2498	.86332	-.00010
0.30	.84049	0.2998	.84060	-.00013
0.35	.81895	0.3497	.81909	-.00018
0.40	.79851	0.3996	.79869	-.00023
0.477	.76889	0.4765	.76913	-.00030
0.50	.76056	0.4997	.76082	-.00034

Slope of G_{E_n} versus q^2 using Gross' correction is
0.0185 ± 0.0022.

Slope of G_{E_n} versus q^2 using Friar's correction is
0.0180 ± 0.0022.

APPENDIX E

COMPUTER PROGRAMS

Six FORTRAN programs were used to perform calculations needed for this work. They are TOPRADCR, TOPROTON, TOPDEUTR, BERHFORM, TRADFORM and BERRELCR. The first three were written by Topping and can be found in Reference [5]. BERHFORM and TRADFORM calculate the experimental cross sections for each of the four channels considered for hydrogen and deuterium respectively. BERHFORM is reproduced on the following pages. BERRELCR was used to compare the relativistic corrections of Gross and Friar.

```
      DIMENSION N(100),M(100),T(100),E(100),X(100),N4(100),N5(100)
      DIMENSION COUNTU(100),CNTVU(100),TNN(100),TNU(100),TNNP(100)
      DIMENSION CONSTA(10),PEAK(100),N6(100),N7(100),SEM(10),NBACK(10)
     1,DD1(90),AA4(90),AA5(90),AA6(90),AA7(90),AAA(30),BBB(30),
     1CCC(30),DDD(30),EEE(30),JAY(10),CRATE(100),AA(30),DD(30)
      REAL LAST
      REAL*8 TITLE(12)
      REAL*4 NUMER,NA,NCAP
      REAL*8 LABEL/'        '/
      READ(5,100)TITLE
  100 FORMAT(6A8)
      DATA EC/1.6E-19/,NA/6.023E23/,NCAP/1.0E-6/
      DO 800 I=4,7
      READ(5,99)FKS,FKB,RHO,TH,A,PSI
      WRITE(6,401)
  401 FORMAT(1HO,'     FKS       FKB        RHO        TH        MCL. MASS  A
     1NGL')
      WRITE(6,99)FKS,FKB,RHO,TH,A,PSI
      NUMER=(EC*FKS*FKB)/(2.0*0.0034877*NCAP)
      DENOM1=(RHO*TH*NA*1.831E-3)
      DENOM2=A*COS(PSI*6.2818/360)
      DENOM=DENOM1/DENOM2
      CONSTA(I)=NUMER/(0.001*DENOM)
      READ(5,103)SEM(I),NBACK(I),CBKG,VBKG,JAY(I)
  103 FORMAT(F10.6,I10,2F10.2,I10)
      WRITE(6,402)I
  402 FORMAT(1HO,'  SEM(',I2,')      NBACK      CBKG       VBKG        JAY')
      WRITE(6,103)SEM(I),NBACK(I),CBKG,VBKG,JAY(I)
  800 CONTINUE
      K=1
      READ(5,90)N4(1),N5(1),N6(1),N7(1),M(1),T(1),H,L,E(1),W,INTU,UMET
      X(1)=INTU/100.0
   90 FORMAT(21X,4I7,31X,/I7,F7.1,F7.2,I7,F7.2,F7.2,I7,F12.2)
      WRITE(6,92)
      WRITE(6,91)H,L,W,UMET
      WRITE(6,92)
      WRITE(6,93)N4(K),N5(K),N6(K),N7(K),M(K),T(K),E(K),X(K)
      K=2
  600 READ(5,101,END=850)N4(K),N5(K),N6(K),N7(K),M(K),T(K),E(K),INTU
      X(K)=INTU/100.0
  101 FORMAT(21X,4I7,31X,/I7,F7.1,15X,F6.2,9X,I5)
      WRITE(6,93)N4(K),N5(K),N6(K),N7(K),M(K),T(K),E(K),X(K)
      K=K+1
      GO TO 600
  850 LIM=K-2
   91 FORMAT(' MACHINE ENERGY=',F7.2,'   VOLT SET:',I7,'   CAPACITOR SET
```

```
     1:',F7.2,'  NORM INT:',F7.2)
   92 FORMAT('  ')
   93 FORMAT(' NO.FOUR   NO.FIVE   NO.SIX    NO.SEVN   BACKING    TIME
     1   SPECT. ENERGY   INT|MV|',/3X,I4,6X,I4,5X,I4,7X,I4,5X,I5,4X,F6.1
     2,6X,F6.2,6X,F6.2)
   95 FORMAT(6F10.6)
C CALCULATE THE INTEGRAL
      DO 1000 IN=4,7
      LIMIT=LIM+1
      IF(IN.EQ.4) GO TO 1100
      IF(IN.EQ.5) GO TO 1200
      IF(IN.EQ.6) GO TO 1300
      DO 20 J=1,LIMIT
      N(J)=N7(J)
   20 CONTINUE
      NC=3
      ITYPE=4
      GO TO 1400
 1100 DO 30 J=1,LIMIT
      N(J)=N4(J)
   30 CONTINUE
      NC=1
      ITYPE=1
      EXSC=300.0
      IXLP=1
      GO TO 1400
 1200 DO 40 J=1,LIMIT
      N(J)=N5(J)
   40 CONTINUE
      NC=2
      ITYPE=2
      GO TO 1400
 1300 DO 50 J=1,LIMIT
      N(J)=N6(J)
   50 CONTINUE
      ITYPE=3
      NC=2
 1400 CONTINUE
      WRITE(6,92)
      WRITE(6,6) IN
    6 FORMAT(28X,' *******HYDROGEN PEAK NUMBER ',I2,'*******')
      WRITE(6,92)
      SUM=0.0
      EBG=(NBACK(IN)*SEM(IN))/(CBKG*VBKG*UMET/300.0)
      DO 550 I=1,LIMIT
      URATE(I)=N(I)/T(I)
      CCUNTU(I)=N(I)/(1-.00097*URATE(I))
      CNTVU(I)=CCUNTU(I)*UMET/X(I)
```

```
      TNU(I)=(CNTVU(I)*SEM(IN))/(W*L*UMET/30.0)
      TNN(I)=TNU(I)-BKG
      WRITE(6,303)I
  303 FORMAT(1HO,'           COUNTU              CNTVU              ENERGY
     1          TNU                BKG        I=',I3)
      WRITE(6,304)COUNTU(I),CNTVU(I),E(I),TNU(I),BKG
  304 FORMAT(8X,F9.4,10X,F9.4,11X,F5.2,12X,F8.6,10X,F8.6)
      WRITE(6,305) LIMIT
  305 FORMAT('      URATE      NUVOLT        TNN              LIMIT=',I4)
      WRITE(6,306) URATE(I),L,TNN(I)
  306 FORMAT(F10.4,3X,I6,F15.6)
      PEAK(I)=CNTVU(I)-NBACK(IN)
      WRITE(6,307)PEAK(I),E(I)
  307 FORMAT(5X,'PEAK =',F8.2,5X,'ENERGY =',F8.2)
  550 CONTINUE
      DO 660 I=1,LIM
      TMP=(TNN(I)+TNN(I+1))*(E(I)-E(I+1))/(E(I)*(1.0+0.0039*(IN-5)))
      WRITE(6,308)I
  308 FORMAT(1HO,'       SUM          TMP                    CONSTA          J
     1=',I4)
      WRITE(6,309)SUM,TMP,CONSTA(IN)
  309 FORMAT(3E16.6)
      SUM=SUM+TMP
  660 CONTINUE
      CROSS=SUM*CONSTA(IN)
      WRITE(6,92)
      WRITE(6,94) CROSS
   94 FORMAT(1HO,'CROSS SECTION =',E16.6)
      WRITE(6,92)
      CNTSUM=0.0
      PARSUM=0.0
      NISUM=0.0
      DO 662 I=1,LIMIT
      NISUM=NISUM+N(I)
  662 CONTINUE
      DO 562 I=1,LIMIT
      PARSUM=CNTVU(I)-NBACK(IN)
      CNTSUM=CNTSUM+PARSUM
      WRITE(6,563) CNTSUM,NISUM
  563 FORMAT( 1HO,'SUM OF HYDROGENIC COUNTS=',F10.2,5X,'TOTAL COUNTS=',I
     110)
  562 CONTINUE
      A=NBACK(IN)/FLOAT(JAY(IN))
      B=LIMIT**2
      BB=A*B
      D=FLOAT(NISUM)+BB
      F=FLOAT(LIMIT)*FLOAT(NBACK(IN))
      EQ=FLOAT(NISUM)-F
```

```
      G=EG**2
      Z=D/G
      STATP=100.0*SQRT(Z)
      WRITE(6,72)STATP
   72 FORMAT(1H0,'STATISTICAL PERCENTAGE DUE TO THE NUMBER OF COUNTS=',F
     110.5)
      DO 888 I=1,LIMIT
      TANP(I)=TAN(I)*1000.0
      BKGP=1000.0*BKG
      WRITE(6,889) BKGP,TANP(I)
  889 FORMAT(2F16.2)
  888 CONTINUE
      N1=1
      N2=30
      IF(N2.GT.LIMIT)N2=LIMIT
      DO 8000 I=N1,N2
      AA(I)=PEAK(I)
      DD(I)=-E(I)
 8000 CONTINUE
      N3=N2+1
      IF(IN.EQ.4) GO TO 9010
      IF(IN.EQ.5) GO TO 9020
      IF(IN.EQ.6) GO TO 9030
      DO 9041 J=N3,LIMIT
      DD1(J-N3+1)=-E(J)
      AA7(J-N3+1)=PEAK(J)
 9041 CONTINUE
      LIM2=LIMIT-N3+1
      GO TO 9042
 9010 DO 9011 J=N3,LIMIT
      AA4(J-N3+1)=PEAK(J)
 9011 CONTINUE
      GO TO 9042
 9020 DO 9021 J=N3,LIMIT
      AA5(J-N3+1)=PEAK(J)
 9021 CONTINUE
      GO TO 9042
 9030 DO 9031 J=N3,LIMIT
      AA6(J-N3+1)=PEAK(J)
 9031 CONTINUE
 9042 NPTS=N2-N1+1
      CALL DRAW(NPTS,AA,DD,MC,ITYPE,LABEL,TITLE,EXSC,0.0,IXUP,1,1,2,9,15
     1,1,LAST)
      WRITE(6,92)
      WRITE(6,92)
 1000 CONTINUE
 1001 N1=1
      N2=30
```

```
      IF(N1.GT.LIM2) GO TO 9800
      IF(N2.GT.LIM2)N2=LIM2
      DO 9700 J=N1,N2
      AAA(J)=AA4(J)
      BBB(J)=AA5(J)
      CCC(J)=AA6(J)
      DDD(J)=AA7(J)
      EEE(J)=DD1(J)
9700  CONTINUE
      IF(N2.EQ.LIM2) GO TO 9750
      DO 9710 J=N1,LIM2
      AA4(J)=AA4(J+N2)
      AA5(J)=AA5(J+N2)
      AA6(J)=AA6(J+N2)
      AA7(J)=AA7(J+N2)
      DD1(J)=DD1(J+N2)
      LIM2=LIM2-N2
9710  CONTINUE
9750  NPTS=N2-N1+1
      IF(NPTS.LT.5) GO TO 9800
      CALL DRAW(NPTS,AAA,EEE,1,1,LABEL,TITLE,EXSC,0.0,IXUP,1,1,2,9,15,1,
     1LAST)
      CALL DRAW(NPTS,BBB,EEE,2,2,LABEL,TITLE,EXSC,0.0,IXUP,1,1,2,9,15,0,
     1LAST)
      CALL DRAW(NPTS,CCC,EEE,2,3,LABEL,TITLE,EXSC,0.0,IXUP,1,1,2,9,15,0,
     1LAST)
      CALL DRAW(NPTS,DDD,EEE,2,4,LABEL,TITLE,EXSC,0.0,IXUP,1,1,2,9,15,0,
     1LAST)
      IF(LIM2.EQ.N2) GO TO 9800
      GO TO 1001
9800  STOP
      END
```

```
      DOUBLE PRECISION RAT,GROSS,FRIAR,PROT2,Q2
      DIMENSION X(100),Y(100)
      READ (5,100) NPTS
  100 FORMAT(I5)
      READ (5,200) (X(I),Y(I),I=1,NPTS)
  200 FORMAT(F10.3,F15.8)
      Q2=0.0475
      DEUT2=(1875.5/197.32)**2.
      PROT2=(938.20/197.32)**2.
      DELT=.0025
      WRITE(6,300)
  300 FORMAT(3X,'Q2',5X,'GROSS REL.',6X,'CE(Q2)',6X,'Q2PRIM',4X,'FRIAR R
     1EL.',4X,'CE(Q2PRIM)',11X,'RELA.',/,1X,'(FM-2)',3X,'CORRECTION',7X,
     2'LF05',7X,'(FM-2)',4X,'CORRECTION',7X,'LF05',14X,'DIFF.')
      DO 800 I=1,221
      Q2=Q2+DELT
      GROSS=(1.-(Q2/8./PROT2))
      FRIAR=1./(1.+Q2/4./PROT2)**.5
      XIN=Q2
      NTERMS=2
      CALL INTERP(X,Y,NPTS,NTERMS,XIN,YOUT)
      CEG=YOUT
      XIN=Q2/(1.+Q2/4./DEUT2)
      NTERMS=2
      CALL INTERP(X,Y,NPTS,NTERMS,XIN,YOUT)
      CEF=YOUT
      RAT=1.-FRIAR/GROSS
      RAT1=1.-CEF/CEG
      WRITE(6,400)Q2,GROSS,CEG,XIN,FRIAR,CEF,RAT,RAT1
  400 FORMAT(  2(F6.4,4X,F10.8,4X,F10.8,4X),E15.8,4X,E15.8)
  800 CONTINUE
      STOP
      END


      SUBROUTINE INTERP(X,Y,NPTS,NTERMS,XIN,YOUT)
      DOUBLE PRECISION DELTAX,DELTA,A,PROD,SUM
      DIMENSION X(100),Y(100),DELTA(20),A(20)
C     C
C     C    SEARCH FOR APPROPRIATE VALUE OF X(1)
C     C
   11 DO 19 I=1,NPTS
      IF(XIN-X(I)) 13,17,19
   13 I1=I-NTERMS/2
      IF(I1) 15,15,21
```

```
   15 I1=1
      GO TO 21
   17 YOUT=Y(I)
   18 GO TO 61
   19 CONTINUE
      I1=NPTS-NTERMS+1
   21 I2=I1+NTERMS-1
      IF(NPTS-I2) 23,31,31
   23 I2=NPTS
      I1=I2-NTERMS+1
   25 IF(I1) 26,26,31
   26 I1=1
   27 NTERMS=I2-I1+1
C
CC    C    EVALUATE DELTA
C
   31 DENOM=X(I1+1)-X(I1)
      DELTAX=(XIN-X(I1))/DENOM
      DO 35 I=1,NTERMS
      IX=I1+I-1
   35 DELTA(I)=(X(IX)-X(I1))/DENOM
C
CC    C     ACCUMULATE COEFFICIENTS A
C
   40 A(1)=Y(I1)
   41 DO 50 K=2,NTERMS
      PROD=1.
      SUM=0.0
      IMAX=K-1
      IXMAX=I1+IMAX
      DO 49 I=1,IMAX
      J=K-1
      PROD=PROD*(DELTA(K)-DELTA(J))
   49 SUM=SUM-A(J)/PROD
   50 A(K)=SUM+Y(IXMAX)/PROD
C
CC    C     ACCUMULATE SUM OF EXPANSION
C
   51 SUM=A(1)
      DO 57 J=2,NTERMS
      PROD=1.
      IMAX=J-1
      DO 56 I=1,IMAX
   56 PROD=PROD*(DELTAX-DELTA(I))
   57 SUM=SUM+A(J)*PROD
   60 YOUT=SUM
   61 RETURN
      END
```

BIBLIOGRAPHY

1. Mader, T. W., Naval Postgraduate School Thesis, (June 1971).

2. Stewart, J. W., Ph.D. Thesis, Naval Postgraduate School, (June 1970). Bumiller, F. A., et al. Phys. Rev. Ltrs. 25, 1774 (1970).

3. Drickey, D. J. and Hand, L. N., Phys. Rev. Ltrs. 9, 521 (1962).

4. Krohn, V. E. and Ringo, G. R., Phys. Rev. 148, 1303 (1966).

5. Topping, R. L., Ph.D. Thesis, Naval Postgraduate School, (December 1972).

6. Gross, F., Phys. Rev. 142, 1025 (1966).

7. Schumacher, C. R. and Bethe, H. A., Nucleon Electromagnetic Structure (to be published).

8. Friar, J. L., private communication.

9. Mott, N. F., Proc. Roy. Soc. (London), A124, 425 (1929).

10. Rosenbluth, M. N., Phys. Rev., 79, 615 (1950).

11. Hand, L. N., Miller, D. G., and Wilson, R., Rev. Mod. Phys. 35, 335 (1963).

12. Lehman, P., Taylor, R., and Wilson, R., Phys. Rev. 126 1183 (1962).

13. Brooks, J. H., and Sessler, G. F., Naval Postgraduate School Thesis, (June 1971).

14. Jankus, V. Z., Phys. Rev. 102, 1586 (1956).

15. Elias, J. E., et al., Phys. Rev. 177, 2075 (1969).

16. Lomon, E. L., private communications.

17. Lomon, E. L., and Feshbach, H., Annals of Physics 48, 94-172 (1968).

18. Casper, B. M. and Gross, F., Phys. Rev. 155, 1607 (1967).

19. deVries, C., Hofstadter, R., Johansson, A., and Herman, R., Phys. Rev. 134, B848 (1964).

20. Källen, G., Elementary Particle Physics, Addison Wesley Reading, Ma. (1964).

21. Sachs, R. G., Phys. Rev. 126, 2256 (1963).

22. Ernst, F. J., Sachs, R. G., and Wali, K. C., Phys. Rev. 119, 1105 (1960).

23. Chodorow, M., et al., Rev. of Sci. Inst. 26, 134 (1955).

24. Barnett, M. T. and Cuneen, W. J., Naval Postgraduate School Thesis (1966).

25. Oberdier, L. D., Naval Postgraduate School Thesis (1966).

26. Schwinger, J., Phys. Rev. 76, 790 (1949).

27. Tsai, Y.-S., Phys. Rev. 122, 1898 (1961).

28. Meister, N. T. and Yennie, D. R., Phys. Rev. 130, 1210 (1963).

29. Maximon, L. C., Medium Energy Nuclear Physics with Electron Linear Accelerators, MIT 1967. Summer Study, edited by W. Bertozzi and S. Kowalski, TID-24667, p. 242 and 249.

30. Bethe, H. and Heitler, W., Proc. Roy. Soc. (London) A146, 83 (1934).

31. Heitler, W., The Quantum Theory of Radiation, Oxford University Press, London (1954).

32. Bethe, H. and Ashkin, J., Experimental Nuclear Physics, Vol. I, edited by Segre John Wiley & Sons, N.Y., N.Y. (1953).

33. Butcher, J. C. and Messel, H., Nuc. Phys. 20, 15 (1969).

34. Landau, L., Soviet J. of Physics VIII No. 4, 201 (1944).

35. Isabelle, D. B. and Bishop, G. R., Nuc Phys. 45, 209 (1963).

36. Börsch-Supan, W., Journal of Research of the National Bureau of Standards 65B, 245 (1961).

37. Air Products and Chemicals, Long Beach, California, private communication.

38. Galster, S., et al., Nuclear Physics B32, 221 (1971).

39. Gourdin, M., Nuevo Cimento 28, 533 (1963), 32, 493 (E) (1964).

INITIAL DISTRIBUTION LIST

		No.Copies
1.	Library, Code 0212 Naval Postgraduate School Monterey, California 93940	2
2.	Defense Documentation Center Cameron Station Alexandria, Virginia 22314	2
3.	Raymond W. Berard 3366 Tennessee St., Apt. 15 Vallejo, California 94590	1
4.	Timothy Traverso 3366 Tennessee St., Apt. 15 Vallejo, California 94590	1
5.	Professor X. K. Maruyama, Code 61Mp Department of Physics Naval Postgraduate School Monterey, California 93940	5
6.	Professor F. R. Buskirk, Code 61Bs Department of Physics Naval Postgraduate School Monterey, California 93940	5

UNCLASSIFIED
Security Classification

DOCUMENT CONTROL DATA - R & D

(Security classification of title, body of abstract and indexing annotation must be entered when the overall report is classified)

1. ORIGINATING ACTIVITY (Corporate author)

Naval Postgraduate School
Monterey, California 93940

2a. REPORT SECURITY CLASSIFICATION

Unclassified

2b. GROUP

3. REPORT TITLE

NEUTRON FORM FACTORS FROM ELASTIC ELECTRON-DEUTERON SCATTERING RATIO EXPERIMENTS AT VERY LOW MOMENTUM TRANSFERS

4. DESCRIPTIVE NOTES (Type of report and, inclusive dates)

Master's Thesis; June 1973

5. AUTHOR(S) (First name, middle initial, last name)

Raymond W. Berard; Ensign, United States Navy
Timothy Joseph Traverso; Ensign, United States Navy

6. REPORT DATE

June 1973

7a. TOTAL NO. OF PAGES

99

7b. NO. OF REFS

39

8a. CONTRACT OR GRANT NO.

b. PROJECT NO.

c.

d.

9a. ORIGINATOR'S REPORT NUMBER(S)

9b. OTHER REPORT NO(S) (Any other numbers that may be assigned this report)

10. DISTRIBUTION STATEMENT

Approved for public release; distribution unlimited.

11. SUPPLEMENTARY NOTES

12. SPONSORING MILITARY ACTIVITY

Naval Postgraduate School
Monterey, California 93940

13. ABSTRACT

Measurements of the ratio of the elastic electron-deuteron scattering cross section to the elastic electron-proton scattering cross section were made for low momentum transfers. Augmented by the work of Topping [5], these data span a range of q^2 from 0.05 fm^{-2} to 0.50 fm^{-2}. From these, the electric form factor of the neutron, G_{E_n}, was extracted using three Lomon-Feshbach wave functions for the deuteron, (LF1, LF5, and LF15). Values of the slope of G_{E_n} versus q^2 were measured to be 0.0218 ± 0.0022 for LF1, 0.0220 ± 0.0022 for LF5, and 0.0185 ± 0.0022 for LF15. Although the data seems to prefer model LF15, all were found to be in agreement with the thermal neutron-electron slope of 0.0193 ± 0.0004. The root mean square structure radius of the deuteron was also extracted, using a method devised by Schumacher, and was found to be 1.9665 ± 0.0045 fm. Relativistic corrections proposed by Casper and Gross [6,18] were compared with the relativistic correction of Friar [8] and no significant differences were found in the region investigated.

DD FORM 1 NOV 1473 (PAGE 1)

S/N 0101-807-6811

UNCLASSIFIED
Security Classification

A-31408

KEY WORDS	LINK A		LINK B		LINK C	
	ROLE	WT	ROLE	WT	ROLE	WT
FORM FACTORS						
NEUTRON						
DEUTERON						
LINAC						

145004
Thesis
B3985 Berard
c.1 Neutron form factors from elastic electron-deuteron scattering ratio experiments at very low momentum transfers.